Cas phosphorylation regulates focal adhesion assembly

Saurav Kumar, Amanda Stainer, Julien Dubrulle, Christopher Simpkins[1] and Jonathan A Cooper[2]

Fred Hutchinson Cancer Center, 1100 Fairview Ave N, Seattle, Washington

[1] Present address: BCMB Program, Johns Hopkins University School of Medicine

[2] Corresponding author: jcooper@fredhutch.org

Abstract

Integrins link the cytoskeleton to the extracellular matrix for cell attachment and migration. Integrin ligation activates tyrosine kinases and stimulates phosphorylation of several integrin-associated proteins. However, the role of such phosphorylation in the assembly of integrin adhesions is unclear. Using spreading or migrating epithelial cells, we provide evidence that phosphorylated Cas (p130Cas, BCAR1), its binding partner, Crk, and inactive focal adhesion kinase (FAK) cluster together with inactive integrins at the cell periphery at sites that subsequently develop into focal adhesions containing F-actin, active integrins, active FAK and core adhesome proteins such as vinculin and talin. Cas, Crk, Src family kinases (SFK) and Rac1 are required for focal adhesion formation and cell spreading. Rac1 provides positive feedback onto Cas through reactive oxygen, opposed by negative feedback from the ubiquitin proteasome system. The results suggest that SFK-Cas-Crk-Rac1 signaling precedes and regulates focal adhesion assembly in epithelial cells.

Introduction

Cell migration is tightly regulated during all stages of metazoan life, from gastrulation to organogenesis, tissue homeostasis and healing in adults (Mayor et al., 2016, Rorth 2011). Deregulated cell migration contributes to pathological states including fibrosis, inflammation, and cancer. Cell attachment to extracellular matrix (ECM) is mediated by heterodimeric α-β integrins, transmembrane proteins that bridge between the ECM and cytoskeleton (Hynes 2002). Integrins switch between closed-inactive and open-active conformations in response to extracellular ligands or binding of intracellular regulatory proteins (Iwamoto et al., 2015, Law et al., 1996, Su et al., 2016). Activated integrins nucleate the assembly of transient protein complexes, known as nascent adhesions or focal complexes, which can grow over time to become larger, more stable, focal adhesions (Iwamoto et al., 2015, Kanchanawong et al., 2022, Moser et al., 2009). At the ultrastructural level, focal adhesions contain nanoclusters of proteins arranged in layers, with integrin tail-associated proteins closest to the membrane, followed by force-transducing talin and vinculin, and F-actin and actin-associated proteins on top (Kanchanawong et al., 2010, Legerstee et al., 2021). Forces generated by actin flow or actomyosin contractility play key roles in focal adhesion assembly. For example, talin is a mechanosensing protein that unfolds under force, exposing binding sites for vinculin and other structural and regulatory proteins, providing additional links to actin stress fibers, building resistance to contractile forces and driving cell translocation (Wolfenson et al., 2019).

While physical forces and mechanosensing explain many aspects of adhesion dynamics, integrins are also signaling receptors. Integrin ligands, including ECM and antibodies, rapidly activate Src-family kinases (SFKs) and focal adhesion kinase (FAK), leading to tyrosine phosphorylation of many integrin-associated proteins including Cas (p130Cas, BCAR1) and paxillin and activating the Rac1 GTPase (Burridge et al., 1992, Harte et al., 1996, Mitra et al., 2006, Miyamoto et al., 1995, Nojima et al., 1995, Parsons et al., 2010, Petch et al., 1995, Vuori et al., 1995, Webb et al., 2002, Zaidel-Bar et al., 2003). Cas is a scaffolding protein that is critical for embryonic development and SFK-mediated cell transformation, regulates cancer in various mouse models, and is associated with poor survival in breast cancer (Cabodi et al., 2010, Honda et al., 1999, Honda et al., 1998, Pylayeva et al., 2009, van der Flier et al., 2000, Wallez et al., 2012, Wendt et al., 2009). At the molecular level, Cas localizes to focal adhesions through an

N-terminal SH3 domain and a C-terminal focal adhesion targeting (FAT) domain (Donato et al., 2010, Nakamoto et al., 1997). SFKs and Cas mutually activate each other, with Cas stabilizing active SFKs and SFKs phosphorylating Cas at up to 15 repeated YxxP motifs (Chodniewicz et al., 2004, Pellicena et al., 2001). After phosphorylation, the pYxxP motifs bind specific SH2-domain proteins including Crk and CrkL. Crk/CrkL in turn bind and stimulate various proteins, including DOCK180, a Rac1 guanine nucleotide exchange factor (GEF) (Chodniewicz et al., 2004, Gotoh et al., 1995, Hasegawa et al., 1996, Klemke et al., 1998, Knudsen et al., 1994, Tanaka et al., 1994). Rac1 can then promote actin polymerization and lamellipodial protrusion through the WAVE/Arp2/3 complex, as well as induce focal complexes through unknown mechanisms (Nobes et al., 1995, Stradal et al., 2004, Zaidel-Bar et al., 2003). Cas phosphorylation also stimulates Cas degradation by the ubiquitin-proteasome system, locally inhibiting Cas signaling (Steenkiste et al., 2021, Teckchandani et al., 2016, Teckchandani et al., 2014).

The role of integrin-activated phosphorylation in focal adhesion assembly is unclear. Some early inhibitor studies suggested that tyrosine kinases were important for adhesion assembly (Burridge et al., 1996). However, studies of mutant mouse embryo fibroblasts (MEFs) showed that SFKs, Cas and FAK are not required for adhesion assembly, instead being critical for adhesion turnover (Bockholt et al., 1995, Webb et al., 2004). To revisit this question in a different cell type, we investigated the kinetics and role of Cas and SFKs in focal adhesion dynamics in epithelial cells during spreading or migration. Unexpectedly, we found that phosphorylated Cas co-clusters with inactive integrins nearly a minute before core focal adhesion proteins join the cluster and integrins are activated. A positive-feedback loop between SFKs, Cas, Crk, Rac1 and reactive oxygen species (ROS) promotes the formation of these early clusters and subsequent adhesion assembly, opposed by negative feedback from the ubiquitin-proteasome system. The results suggest a key role for SFK-Cas-Crk-Rac1 signaling in early stages of focal adhesion formation.

Results

Live imaging shows Cas clusters mark sites of future vinculin clusters

Live imaging of migrating mouse fibroblasts revealed that tyrosine phosphorylation occurs early during nascent adhesion formation (Zaidel-Bar et al., 2003). Integrin clustering induces rapid recruitment and phosphorylation of Cas, FAK and paxillin (Miyamoto et al., 1995). To determine the kinetics of Cas recruitment and activation in a different cell type, we turned to an immortalized epithelial cell line, MCF10A. These cells have been used as a cancer model, and to study adhesion dynamics during single-cell and collective migration (Beckham et al., 2014, Debnath et al., 2005, Teckchandani et al., 2016). Since Cas over-expression stimulates cell migration (Klemke et al., 1998, Yano et al., 2000), we used genome editing to express fluorescently tagged Cas at endogenous level, inserting an artificial exon encoding mScarlet (mSc) into the first intron of the *Cas* gene (Figure 1A, Figure 1 –figure supplement 1A). Genome sequencing provided evidence for different clones with varied indels at the insertion site, but these errors were corrected by splicing, yielding an mRNA encoding the expected Cas^{mSc} fusion protein (Figure 1 –figure supplement 1B-E). Western blotting revealed similar levels and phosphorylation of Cas and Cas^{mSc} proteins, indicating that most cells are heterozygous (Figure 1B). This intron tagging approach avoided the need for single-cell cloning that can select for variants (see Methods).

To test whether Cas^{mSc} localizes to focal adhesions, Cas^{mSc} cells were transduced to express near-endogenous levels of YFP-tagged vinculin (VCL) and imaged using total internal reflection (TIRF) microscopy. Cas^{mSc} and YFP-VCL substantially co-localized (Figure 1C). To compare Cas^{mSc} and YFP-VCL dynamics, we performed dual-channel time-lapse TIRF imaging as cells attached and spread on a collagen I-coated surface. Cas^{mSc} formed clusters at the first points of cell-substrate contact and moved outwards with the spreading edge (Figure 1D, Supplementary Video 1). Vinculin clusters formed later, often overlapping with Cas clusters. Kymographs revealed sites where Cas clusters developed into vinculin clusters (Figure 1D, note transition from magenta to white to green). Similar patterns of Cas and vinculin clustering were observed under spontaneous lamellipodial protrusions generated by fully spread cells (Figure 1E, Supplementary Video 2). Again, kymographs revealed many Cas clusters that developed into

vinculin clusters (Figure 1E). These results together suggest that Cas clusters mark sites of future vinculin clusters during spreading and migration.

To quantify the dynamics of cluster formation and avoid possible selection bias, we developed a computational pipeline to delineate regions of interest (ROIs) in which Cas, vinculin, or both Cas and vinculin intensities exceeded thresholds that were automatically set for each frame (see Methods). ROIs were tracked over time and quantified if they exceeded 20 pixels in area (0.5 μm^2) and persisted for at least 3 frames ($\geq$40 s) (Figure 1F, Supplementary Video 3). These thresholds exclude the smallest, shortest-lived nascent adhesions but include larger focal complexes (Kanchanawong et al., 2022). The mean intensity of each channel in each ROI was then quantified over the duration of the recording and the intensities smoothed and normalized to a range of 0 to 1 (Figure 1 – figure supplement 2A). Profiles of individual ROIs showed a strong trend for Cas intensity to increase before vinculin intensity and for Cas intensity to decrease before vinculin intensity. We measured the time delay between Cas and vinculin reaching half-maximal intensity, $\Delta t_{1/2}$ (VCL-Cas) (Figure 1 – figure supplement 2B). Time delays for ROIs in a single cell varied with a non-normal distribution (Figure 1 – figure supplement 2C). However, the probability of vinculin joining a Cas cluster was much greater than Cas joining a vinculin cluster, with median $\Delta t_{1/2}$ (VCL-Cas) significantly greater than zero (median 54.8 s, 95% CI 23-105 s, for 90 ROIs in the cell shown) (Figure 1 – figure supplement 2C). This bolsters the hypothesis that Cas is a leading indicator for ensuing vinculin dynamics. Averaging the median $\Delta t_{1/2}$ (VCL-Cas) across 19 spreading cells in several experiments yielded a time delay of 43.8$\pm$3 s (mean and SEM) (Figure 1G). A broad range of $\Delta t_{1/2}$ (VCL-Cas) was also observed under lamellipodia formed by a migrating cell (Figure 1 – figure supplement 2D). Averaging median $\Delta t_{1/2}$ (VCL-Cas) across multiple ROIs under lamellipodia in 13 migrating cells in several experiments yielded a time delay 68.5$\pm$7 s (mean and SEM) (Figure 1H). Vinculin clustering was also delayed relative to Cas in spreading Cas^{mSc} YFP-VCL HeLa cells (mean $\Delta t_{1/2}$ (VCL-Cas) 44.1$\pm$9 s, Figure 1 – figure supplement 2E-F).

Overall, these results show a strong tendency for Cas to form clusters at the edge of spreading or migrating epithelial cells, 45-60 s before being joined by vinculin. For comparison, the time interval between arrival of talin, vinculin and paxillin in nascent adhesions of CHO-K1 cells

migrating on fibronectin is ~14 s or ~2 s for non-maturing or maturing adhesions respectively (Han et al., 2021). The replacement of Cas clusters by vinculin clusters suggests that Cas may spatially coordinate vinculin clustering and adhesion assembly in both spreading and migrating MCF10A and HeLa cells.

Cas clusters precede vinculin clusters independent of ECM

Cells bind to different matrix proteins through distinct integrin heterodimers, such as α5β1 for fibronectin and α2β1 for collagen (Hynes 2002). To test whether Cas clusters co-localize with focal adhesions formed by different integrins, we seeded Cas^{mSc} YFP-VCL MCF10A cells on different matrix proteins (Figure 2A). Cell spreading on fibronectin was inhibited by the integrin α5β1-blocking monoclonal antibody (mAb) P8D4 (Alfandari et al., 2003, Davidson et al., 2002), while spreading on collagen was inhibited by the integrin α2β1-blocking mAb P1E6 (Carter et al., 1990, Tuckwell et al., 1995) (Figure 2A). Mature adhesions, detected with the conformation-specific 9EG7 mAb that binds active integrin β1 (Bazzoni et al., 1995, Lenter et al., 1993), were larger and more intense on collagen than fibronectin (Figure 2B). Nevertheless, TIRF imaging of the ventral surface of cells attaching and spreading on fibronectin showed a similar clustering of Cas before vinculin (Supplementary Video 4). The mean $\Delta t_{1/2}$ (VCL-Cas) was similar for fibronectin and collagen (Figure 2C), suggesting Cas clusters may specify localization of integrin α5β1 and α2β1 adhesions.

Initial Cas clusters mark sites of future integrin clusters

To test whether integrins localize to early or late Cas clusters, we transduced MCF10A Cas^{mSc} cells with a lentiviral vector encoding β1Ecto-pH, a recombinant integrin β1 with a pH-sensitive pHlorin tag inserted in the extracellular domain (Huet-Calderwood et al., 2017). This integrin is cell-surface expressed, localizes to adhesions, exhibits normal integrin activation, and restores adhesion in integrin β1 knockout MEFs (Huet-Calderwood et al., 2017). Live dual-color TIRF imaging of β1Ecto-pH in Cas^{mSc} MCF10A cells revealed that β1Ecto-pH localized to Cas clusters, but, like YFP-VCL, β1Ecto-pH kinetics were significantly delayed relative to Cas, with mean $\Delta t_{1/2}$ (β1-Cas) 67.33$\pm$9.4 s (Figure 3A-B, Supplementary Video 5 left).

As an independent approach to measure integrin clustering, we edited the *ITGB1* gene in HeLa Cas^{mSc} cells (Figure 3C). Briefly, we targeted the *ITGB1* final intron to insert an artificial exon encoding the C-terminus of integrin β1 fused to GFP through an optimized 18-residue linker (Parsons et al., 2008), followed by the SV40 virus 3' processing and polyadenylation (pA) signal (Figure 3 – figure supplement 1A). Primary transcripts were expected to terminate at the inserted pA signal and be spliced to create an mRNA encoding C-terminally tagged $ITGB1^{GFP}$. Following transfection and FACS, the correct integration and mRNA sequence were confirmed by PCR and RT-PCR (Figure 3 – figure supplement 1B-E). Western blotting with GFP antibody showed a fusion protein of the expected mobility (Figure 2D). Live imaging Cas^{mSc} $ITGB1^{GFP}$ cells revealed integrin clustering after Cas with $\Delta t_{1/2}$ (ITGB1-Cas) 62.9$\pm$7.2 s (mean and SEM, n=11 cells) (Figure 3E-F, Supplementary Video 5 right). Thus, integrin β1 and vinculin are similarly delayed in their arrival in Cas clusters in MCF10A and HeLa cells.

Initial Cas clusters contain Crk

Previous studies showed that integrin clustering or activation by ECM or antibodies stimulates the tyrosine phosphorylation of Cas and other proteins (Arias-Salgado et al., 2003). Our finding that early Cas clusters before integrin led us to wonder whether Cas phosphorylation occurs late in the process. Since Cas phosphorylation cannot be imaged directly, we instead analyzed the recruitment of Crk, which binds phosphorylated but not non-phosphorylated Cas and initiates downstream signaling (Chodniewicz et al., 2004). We edited the *CRK* gene in Cas^{mSc} HeLa cells, targeting the last intron to create a C-terminal fusion of Crk to mGreenLantern (mGL) (Figure 4A, Figure 4 – figure supplement 1A). Following transfection and FACS, the expected integration was confirmed by PCR (Figure 4 - figure supplement 1B-D). Western blotting showed approximately equal expression of Crk^{mGL} and Crk, suggesting most cells are heterozygous (Figure 4B). Imaging Cas^{mSc} Crk^{mGL} cells during attachment and spreading revealed rapid recruitment of Crk^{mGL} on Cas^{mSc} clusters (Supplementary Video 6 left, Figure 4C). The median time delay, $\Delta t_{1/2}$ (Crk-Cas), averaged across several cells, was 5$\pm$3.9 s (Figure 4D), much shorter than the time for vinculin or integrin recruitment. Crk recruitment was significantly delayed by treatment with eCF506, which inhibits all SFKs but not other kinases, indicating that Crk recruitment requires phosphorylation (Supplementary Video 6 right, Figure 4E) (Fraser et al., 2016). Together these results suggest Cas is phosphorylated and recruits Crk

before peak recruitment of integrin and vinculin, raising the possibility that Cas phosphorylation is stimulated by Cas clustering when local integrin density is submaximal.

Spatial distribution of adhesion proteins in Cas clusters

Time-lapse TIRF imaging of spreading Cas^{mSc} YFP-VCL cells showed the continual addition of Cas^{mSc} near the outer edge of the cell, at the head of developing clusters, followed by recruitment of YFP-VCL towards the tail of the cluster (Figure 5A). Thus, the spatial distribution of Cas^{mSc} and YFP-VCL along the length of a cluster reflects their temporal order of assembly. We reasoned that we could estimate the order of arrival and departure of other adhesion proteins from their spatial distribution within Cas clusters. To this end, we fixed and permeabilized Cas^{mSc} YFP-VCL cells after 30 min of spreading and used combinations of different antibodies for TIRF or confocal immunofluorescence imaging. For each antibody combination, intensity profiles were quantified along the length of approximately 20, 4 μm-long clusters from several cells, aligned relative to Cas^{mSc}, normalized, and averaged. Mean normalized intensity profiles of Cas^{mSc} and YFP-VCL are presented in Figure 5B, and results for various antibodies are presented as heat maps in Figure 5C and sample images in Figure 5 – figure supplement 1.

The intensity profiles show several important features. First, phosphorylated (pY410) Cas is maximal at the head of the cluster, ~0.5 μm from the cell edge (Figure 5C, Figure 5 – supplement 1), consistent with the rapid recruitment of Crk^{mGL} to Cas^{mSc} clusters (Figure 4C). The head of the cluster also contained highest amounts of FAK phosphorylated at Y861, an SFK phosphorylation site (Eliceiri et al., 2002). However, levels of FAK protein and kinase-active pY397 FAK (Le Coq et al., 2022), were low at the head of the cluster.

Second, the head of the cluster also contains peak levels of inactive integrin β1, detected with antibody AIIB2 (Takada et al., 1993), suggesting it is not attached to the ECM (Figure 5C, Figure 5 – supplement 1). In contrast, active integrin β1, detected with antibody 9EG7, peaked with YFP-VCL further back in the cluster, ~1.2 μm from the edge. This region also contained highest levels of mechanosensing and structural components of focal adhesions, including kindlin2, talin1, paxillin, kinase-active pY397 FAK and F-actin, but decreased amounts of phosphorylated and total Cas (Figure 5C). The presence of mechanosensing proteins and active

integrins suggests that the center of the cluster is attached to the ECM and subject to mechanical force.

Overall, while differential antibody access may affect immunofluorescent staining profiles, the spatial patterns suggest a temporal sequence of events in which active phosphorylated Cas initially clusters with inactive integrin β1 and SFK-phosphorylated but kinase-inactive FAK. Since integrin β1 is in its closed conformation it is probably not attached to the ECM. Later, phosphorylated and total Cas levels decrease as integrin β1 adopts the active conformation, binds to ECM, resists force, and recruits mechanosensing proteins to form a mature focal adhesion (model, Figure 5D).

Phosphorylated Cas is enriched in the adhesome

Even though many imaging studies have detected Cas in focal adhesions, Cas is not a member of the consensus adhesome as defined by proteomics or proximity biotinylation (Kanchanawong et al., 2022). However, pY Cas is detected in the phosphoadhesome and total Cas could escape detection if its overall abundance is low (Cas protein copy number is ten-fold lower than integrin β1 in MCF10A and HeLa cells (Kulak et al., 2014, Ly et al., 2018)). We used Western blotting as a sensitive approach to characterize the MCF10A cell adhesome. Cells were seeded on polylysine or collagen for 60 min and incubated with protein-protein cross-linking reagents before lysis and separation of adhesome and supernatant fractions as described (Humphries et al., 2009, Schiller et al., 2011). We then reversed the cross-links and performed Western blotting on the adhesome and supernatant samples. This semi-quantitative approach allowed an estimation of the distribution of each protein between the adhesome and supernatant fractions regardless of abundance. We found that the adhesome contained ~20-27% of total cellular integrin β1, talin, vinculin, paxillin, FAK and active (pY397) FAK, but only ~7% of a control protein, ERK (Figure 5 – figure supplement 2). The adhesome fraction also contained ~25% of total cellular Cas, suggesting it is as enriched in adhesions as bona fide adhesion proteins. Moreover, the adhesome fraction of cells plated on collagen but not polylysine contained 73% of total cellular phospho-Cas. This suggests that the subpopulation of Cas in the adhesome is phosphorylated and able to signal while Cas in the cytosol is mostly inactive. Given that most of the Cas in mature adhesions exchanges with the cytosol on a timescale of a few seconds (Machiyama et al., 2014),

Cas may be rapidly phosphorylated when it enters adhesions and dephosphorylated when it leaves while pY397FAK remains active in the cytosol.

Cas regulates vinculin recruitment and focal adhesion assembly

The early arrival of Cas at sites of future focal adhesions suggests it may be regulatory. To test this possibility, we depleted Cas from MCF10A Cas^{mSc} YFP-VCL cells using siRNA (Figure 6 – figure supplement 1A). Cas-depleted cells were non-migratory and their adhesions were immobile (Figure 6 – figure supplement 1B, Supplementary Video 7). Initial cell attachment and spreading were strongly inhibited, with significant decreases in cell area, the number of vinculin clusters, and intensities of Cas, vinculin, and other focal adhesion proteins including talin1, kindlin2 and FAK in the remaining clusters (Figure 6A-B, Figure 6 – figure supplement 1C). By way of comparison, vinculin depletion had little effect on cell spreading, the number of Cas clusters, or the intensity of Cas in those clusters (Figure 6A, B, Figure 6 – figure supplement 1D). This suggests that Cas is limiting for cell spreading, vinculin recruitment and focal adhesion formation but vinculin is not limiting for Cas recruitment, consistent with their order of assembly.

FAK is important to recruit Cas to the edge of spreading fibroblasts (Zhang et al., 2014). FAK is also detected in early Cas clusters in MCF10A cells (Figure 5C). However, depleting FAK had no effect on MCF10A cell spreading, the intensity of Cas or vinculin clusters, or the median time delay between Cas and vinculin recruitment (Figure 6 – figure supplement 2A-C). Kindlin2 and talin1 directly bind integrin tails and play important roles in integrin adhesion in fibroblasts, with kindlin2 interacting with paxillin and talin1 recruiting vinculin and providing attachment for actin, enabling force generation, adhesion maturation and cell spreading (Kanchanawong et al., 2022). Similarly, in MCF10A cells, both kindlin2 and talin1 were important for attachment and spreading. Depleting kindlin2 or talin1 had no effect on Cas clustering, but depleting talin1 decreased cell spreading and the intensity of vinculin clusters, and depleting either kindlin2 or talin1 increased the time delay between Cas and vinculin recruitment (Figure 6 – figure supplement 2D-F). Thus Cas regulates cell spreading and clustering of talin1, kindlin2 and vinculin, and promotes talin1- and kindlin2-dependent recruitment of vinculin.

Integrins can be activated "inside-out" by proteins binding to their cytoplasmic tails, or "outside-in" by interactions with the ECM or with molecules or ions that stabilize the active open conformation (Hynes 2002). We tested whether Cas is required for outside-in adhesion assembly by treating control or Cas-depleted cells with Mn^{2+}, which stabilizes the active integrin conformation (Gailit et al., 1988, Lenter et al., 1993). While Mn^{2+} increased the spread area of control cells, it had no effect on the spreading of Cas-depleted cells and did not rescue the intensity of vinculin clusters (Figure 6C). This suggests that Cas is rate-limiting for outside-in as well as inside-out integrin activation.

SFK-Cas-Crk-Rac1 signaling regulates adhesion assembly

Known Cas signaling pathways involve Cas binding to SFKs through the proline region and pYDYV motif, followed by phosphorylation of the repeated YXXP motifs in the substrate domain and recruitment of various downstream effectors through adaptor proteins such as Crk and CrkL (Chodniewicz et al., 2004). We investigated whether Cas phosphorylation and Crk/CrkL binding are involved in vinculin recruitment in MCF10A Cas^{mSc} YFP-VCL cells by use of the SFK inhibitor eCF506 and RNAi. Either inhibiting SFKs or depleting Crk/CrkL approximately doubled the time interval between Cas and vinculin clustering, suggesting phosphorylation-dependent Cas-Crk/CrkL signaling regulates the rate of focal adhesion formation (Figure 7A, Figure 7 – figure supplement 1A-B, Supplementary Video 8). To test whether a specific SFK regulates adhesion assembly, we knocked down each of the major SFKs - Src, Fyn and Yes1 - and measured adhesion and spreading on collagen. Remarkably, cell spreading, adhesion number, vinculin intensity, and Cas phosphorylation were all inhibited by depletion of Yes1 but not Src or Fyn, while Cas cluster formation was normal (Figure 7B, Figure 7 – figure supplement 1B-D). This implies that Yes1 may have a special role in phosphorylating Cas and recruiting Crk/CrkL to stimulate adhesion assembly in MCF10A cells spreading on collagen.

Crk/CrkL bridge between phosphorylated Cas and downstream effectors including DOCK180-ELMO, which serve as guanine nucleotide exchange factors (GEFs) for Rac1 (Chodniewicz et al., 2004). Rac1 regulates lamellipodia protrusion by binding the WAVE regulatory complex (WRC) to drive Arp2/3 complex-mediated actin polymerization (Takenawa et al., 2007).

Transient activation of Rac1 also induces formation of nascent adhesions at the cell edge, although the specific mechanism is unclear (Nobes et al., 1995, Zaidel-Bar et al., 2003). We used a Forster resonance energy transfer (FRET) biosensor (Rac1-2G) to measure Rac1 activity during MCF10A cell adhesion (Fritz et al., 2015). Rac1-2G FRET activity was stimulated around the periphery of cells attaching to collagen and was inhibited by the Rac1-specific inhibitor EHT1864 (Onesto et al., 2008) (Figure 7 – figure supplement 1E). EHT1864 also inhibited cell spreading and reduced and delayed vinculin clustering but had no effect on Cas clustering (Figure 7C, Figure 7 – figure supplement 1F, Supplementary Video 9 top). Importantly, depleting Cas or Yes1 inhibited Rac1 (Figure 7D-E), consistent with Rac1 activation by the SFK-Cas-Crk/CrkL-DOCK180/ELMO pathway (Chodniewicz et al., 2004). Together, these results suggest that early clustering of phosphorylated Cas with Crk and inactive integrins activates Rac1 to trigger both cell spreading and assembly of vinculin-containing focal adhesions.

Linkage between cell spreading and adhesion assembly through positive and negative feedback

If the sole function of Cas in focal adhesion assembly is to activate Rac1, then activation of Rac1 may bypass the need for Cas. To test this possibility, we over-expressed either wildtype or constitutively-active GFP-Rac1^{Q61L} in MCF10A Cas^{mSc} cells by transient transfection and examined cells during attachment to collagen. As expected, GFP-Rac1^{Q61L} cells spread more than GFP-Rac1^{WT} cells (Figure 8A). Surprisingly, Cas depletion prevented Rac1-induced spreading (Figure 8A). This suggests that, even though Cas requires Rac1 to support normal spreading and adhesion formation, active Rac1 requires Cas to induce spreading, raising the possibility of a positive feedback loop from Rac1 back to Cas.

We investigated which Rac1 effector may be involved in positive feedback on Cas. Rac1 stimulates localized production of reactive oxygen species (ROS) by the Nox1 NADPH-dependent oxidase by binding p47^{phox} (Ushio-Fukai 2006). ROS are short-range signaling molecules, rapidly reacting with and inhibiting protein-tyrosine phosphatases (PTPs) and increasing local tyrosine phosphorylation of various substrates including Cas, SFKs, and p190RhoGAP (Garton et al., 1996, Giannoni et al., 2005, Nimnual et al., 2003, Tonks 2005).

Thus, Rac1 potentially activates Cas through a Rac1-ROS-PTP-SFK-Cas pathway. Such a positive feedback loop, where the output signal is fed back as input, can amplify the signal, enhancing the outcome (Brandman et al., 2008). To test whether ROS are involved in positive feedback and adhesion assembly in MCF10A cells, we inhibited Nox1 with diphenylamineiodonium (DPI) (Reis et al., 2020). DPI inhibited Rac1 (Figure 8B), inhibited cell spreading, and delayed vinculin recruitment to Cas clusters (Figure 8C, Supplementary Video 9). This suggests that positive feedback through ROS amplifies and sustains SFK-Cas-Crk/CrkL-Rac1 activity that recruits vinculin.

Positive feedback loops require negative feedback to avoid runaway amplification (Brandman et al., 2008). Phosphorylation-dependent signaling can be inhibited by PTPs or phosphorylation-dependent proteolysis. During collective migration, Cas signaling is inhibited by negative feedback through the $CRL5^{SOCS6}$ ubiquitin ligase complex, which targets only the phosphorylated form of Cas for proteasomal degradation (Teckchandani et al., 2016, Teckchandani et al., 2014). We tested whether $CRL5^{SOCS6}$ regulates focal adhesion assembly during MCF10A cell attachment. Either SOCS6 depletion or a Cullin inhibitor, MLN4924, shortened $\Delta t_{1/2}$ (VCL-Cas) during cluster assembly, consistent with $CRL5^{SOCS6}$ interfering with focal adhesion formation by negative feedback on phospho-Cas signaling (Figure 8D, Supplementary Video 10).

Together, these results suggest a model in which nascent clusters of inactive integrins, phosphorylated Cas, active SFKs and Crk stimulate Rac1 and generate ROS, creating positive feedback that strengthens and maintains signaling, leading to recruitment of talin1, kindlin2, vinculin and other mechanosensing proteins to form a focal adhesion (Figure 8E). Negative feedback from $CRL5^{SOCS6}$, which ubiquitinates phosphorylated Cas, fine-tunes signal strength to ensure proper assembly.

Discussion

The current view of integrin activation and focal adhesion assembly, based largely on studies in fibroblasts, is that mechanosensitive proteins kindlin2 and talin1 bind to and stabilize active integrins, allowing engagement with rearward flowing actin, recruiting vinculin and opening additional binding sites to build the adhesion and generate high ECM traction force (Henning Stumpf et al., 2020, Kanchanawong et al., 2010, Legerstee et al., 2021, Wolfenson et al., 2019, Zhu et al., 2021). The structural components of focal adhesions are recruited in a timespan of a few seconds (Bachir et al., 2014, Choi et al., 2008, Han et al., 2021, Laukaitis et al., 2001). Phosphorylation is stimulated early in the process (Zaidel-Bar et al., 2003), possibly driven by integrin clustering, which could promote trans-phosphorylation of SFKs (Arias-Salgado et al., 2003, Buensuceso et al., 2003, Huang et al., 1993), or by forces between focal complexes and the cytoskeleton (Pelham et al., 1997, Schoenwaelder et al., 1999). Many manipulations that increase tyrosine phosphorylation also stimulate focal adhesion assembly (Burridge et al., 1996). However, the exact roles of tyrosine kinases, their substrates, and Rac1 in adhesion assembly has remained unclear. Focal adhesion assembly rates were reportedly normal in Cas, FAK and SFK knockout MEFs and Cas is not part of the core adhesome (Horton et al., 2015, Robertson et al., 2015, Webb et al., 2004). In addition, RhoA, not Rac1, is thought to stimulate local actin polymerization for focal complex formation (Kanchanawong et al., 2010, Wolfenson et al., 2019). Our results suggest a different process for adhesion assembly, at least in epithelial cells, with critical roles for SFKs, Cas and Rac1 to recruit mechanosensing proteins (Figure 8E). We find that Cas, Crk, and low amounts of integrin β1 and FAK cluster together at sites that develop into focal adhesions. Moreover, Cas, Crk/CrkL, SFKs and Rac1 are required for focal adhesion assembly. Vinculin, FAK, kindlin2 and talin1 do not regulate Cas clustering. Instead, kindlin2 and talin1 appear to be rate limiting after Cas clustering to recruit vinculin. Integrin β1 is inactive in the early Cas clusters, suggesting it is not engaged with the ECM. Nevertheless, Cas is phosphorylated and associated with Crk. Cas clusters grow through positive feedback involving SFKs, Cas, Crk/CrkL, Rac1 and ROS, opposed by negative feedback through $CRL5^{SOCS6}$. Subsequently, Cas levels and phosphorylation in the clusters decrease as more integrin β1 and core focal adhesion proteins are recruited and activated. Only during this later stage is FAK activated, consistent with FAK as a mechanosensor (Le Coq et al., 2022). Thus, in

epithelial cells, Cas is phosphorylated before integrins are activated, and phospho-Cas signaling is needed to initiate focal complexes and start recruiting mechanosensing proteins.

A central role for Cas in focal adhesion assembly is unexpected but may be cell type- or integrin-specific. Previous studies that identified key roles for kindlin2 and talin1 made use of fibroblasts binding to fibronectin or blood cells interacting with fibrinogen. Fibroblasts bind fibronectin through integrin αvβ3 as well as α5β1, while blood cells bind fibrinogen through αIIbβ3. Integrins may differ in their downstream signaling. For example, talin1 binds more strongly to β3 than to β1 (Anthis et al., 2010, Lu et al., 2016). We found that Cas regulates MCF10A cell adhesion to collagen and fibronectin through integrin α2β1 and integrin α5β1 respectively. β3 integrins may not be involved because MCF10A and HeLa cells express 10-fold less integrin β3 than β1 (Kulak et al., 2014, Ly et al., 2018). There is precedent for integrin-specific requirements for different SFKs. In fibroblasts, Src co-localizes with, and is required for, αvβ3 adhesions but not α5β1 adhesions (Felsenfeld et al., 1999), while Fyn and Cas are needed for force-dependent adhesion assembly mediated by integrin αvβ3 on fibronectin (Kostic et al., 2006, von Wichert et al., 2003). In our experiments, Yes1 was limiting for vinculin recruitment during α2β1-mediated attachment to collagen. SFKs vary in their trafficking mechanisms and affinity for different types of membranes (Resh 1999, Sandilands et al., 2008). Yes1 has a higher affinity than Src for integrin β1 cytoplasmic tails (Arias-Salgado et al., 2003) and for liquid-ordered membrane domains associated with integrin clusters (Lietha et al., 2020). Thus, Yes1 may have specific roles in α2β1-mediated adhesions based on its interactions with membrane microdomains.

Even though we only studied epithelial cells, there are indications that Cas also regulates focal adhesion assembly in fibroblasts. Meenderink et al found that expressing wildtype Cas at normal level in Cas-knockout MEFs doubled the rate of adhesion assembly (Meenderink et al., 2010). This was unexpected given that adhesion assembly rates in wildtype and SFK- or Cas-knockout MEFs were previously reported to be equal (Webb et al., 2004). One possibility is that culturing mutant MEFs as monolayers may select for variant cells with strong adhesion, bypassing a requirement for Cas. We avoided potential selection artifacts by use of transient knockdowns, complemented where possible by chemical inhibitors only during cell spreading or migration.

Other researchers reported that chemogenetic induction of Src-Cas complexes but not Src-FAK complexes in fibroblasts is sufficient to drive adhesion assembly (Karginov et al., 2010). Furthermore, Cas localizes adjacent to new adhesion sites at the edge of spreading fibroblasts (Zhang et al., 2014). However, a potential role for Cas in specifying adhesion localization in fibroblasts was not investigated.

We note that SFK-Cas-Crk/CrkL-Rac1-ROS signaling not only initiates focal adhesion formation but also cell spreading. It was not possible to test whether Cas induces adhesion assembly and spreading through parallel or sequential pathways because of positive feedback: inhibiting any step in the loop inhibited both adhesion assembly and spreading. This makes it challenging to identify the step that simulates adhesion assembly. However, Rac1-induced actin polymerization may drive adhesion assembly, for example by creating retrograde actin flow and activating mechanosensing proteins. Indeed, seminal studies showed that transient expression of active Rac1 induces focal complexes, but these only mature into focal adhesions if RhoA is activated (Nobes et al., 1995). Thus, the loss of Cas from clusters may be important to locally decrease Rac1 activity and allow focal adhesion maturation. Unfortunately, the Rac1 sensor we used did not allow high resolution imaging of Rac1 activity at the level of individual adhesions.

Our results raise the question of how Cas clusters form and grow. Even though integrin β1 density is lower in initial Cas clusters than in later focal adhesions, inactive integrin β1 was readily detected with antibody to inactive β1. Given that integrin β1 is 10-times more abundant than Cas in these cells (Kulak et al., 2014, Ly et al., 2018), there may be similar numbers of inactive integrin β1 and Cas molecules in the initial clusters, and integrin-Cas interaction may somehow initiate clustering. However, direct Cas-integrin binding has not been detected. The Cas SH3 and FAT domains respectively bind focal adhesion proteins FAK and vinculin (Janostiak et al., 2014, Polte et al., 1995) and paxillin, ajuba and BCAR3 (Mace et al., 2011, Pratt et al., 2005, Zhang et al., 2017). However, vinculin, paxillin and FAK were not limiting for Cas clustering in our experiments. Alternatively, as mentioned above, Yes1 may not only phosphorylate Cas but also regulate Cas localization to liquid-ordered membrane domains that contain β1 integrins (Lietha and Izard 2020). Growth of initial clusters could then be driven by networks of phospho-Cas with Crk, CrkL and multivalent downstream effectors, such as

DOCK180. Indeed, recent studies elegantly showed that phospho-Cas undergoes phase separation when mixed with an SH2-SH3 protein, Nck, and an Nck-binding protein, N-WASP (Case et al., 2022). These protein condensates synergize with FAK-paxillin condensates and kindlin to cluster integrins in vitro. While our results differ regarding the specific proteins involved, it is possible that similar protein condensates form from multivalent networks of phospho-Cas with adaptors, effectors and integrins. These condensates could then grow in space and time through Rac1-induced actin polymerization, trans-phosphorylation of Cas-Yes complexes, and positive feedback through ROS. Further understanding of the precise mechanism will require additional in vivo and in vitro analysis.

Materials and Methods

Plasmids

pMSCVpuroEYFPvinculin was described previously (Teckchandani et al., 2016). EGFP-Rac1^{WT} and EGFP-Rac1^{Q61L} were gifted by K. Wennerberg, University of North Carolina, Chapel Hill, NC (Arthur et al., 2004). The following vectors were provided by the indicated investigators: pmScarlet-i_C1 (gifted from Dorus Gadella, Addgene plasmid # 85044), pORANGE cloning template vector (gifted from Harold MacGillavry, Addgene # 131471), pCE-mp53DD (gifted from Shinya Yamanaka, Addgene # 41856), pLenti-Rac1-2G (gifted from Olivier Pertz, Addgene # 66111), pcDNA3.1-mGreenLantern (gifted from Gregory Petsko, Addgene # 161912) (Campbell et al., 2020), pMD2.G and psPAX2 (Didier Trono, Addgene #12259 and 12260). pLenti Ecto-pHluorin β1 integrin with 4-residue linkers was kindly provided by David A. Calderwood (Yale University School of Medicine, USA) (Huet-Calderwood et al., 2017).

Gene editing

We inserted fluorescent protein tags into endogenous genes by homology-independent intron targeting (Serebrenik et al., 2019, Zhong et al., 2021), with modifications. Intron targeting has several advantages over exon targeting. First, the exact position of artificial exon within the intron is unimportant, allowing insertion at the single guide RNA (sgRNA) SpCas9 target site with highest predicted efficiency. Second, the exon does not need to be inserted precisely, since errors should be corrected by RNA splicing. Thus, homology arms are unnecessary, shortening the donor sequence. Third, by inserting a fluorescent protein open-reading frame lacking an initiation codon, the majority of fluorescent cells should be correctly targeted and can be isolated by FACS without need for single-cell cloning.

We used the pORANGE vector which encodes, on a single plasmid, an sgRNA, SpCas9, and a polylinker for subcloning the donor sequence (Willems et al., 2020). Target sites were identified in introns of interest using the CHOPCHOP sgRNA designer (Labun et al., 2019). Corresponding sgRNA sequences were synthesized (Integrated DNA Technologies), annealed and inserted into pORANGE using combined restriction digestion and ligation at the BbsI sites. Donor sequences were then inserted at the HindIII (5') and XhoI or BamHI at (3') sites. For N-

terminal tagging, the donor contained: (a) a canonical splice acceptor (SA) sequence (Smith 1997); (b) a fluorescent tag sequence, lacking initiation codon; (c) a canonical splice donor (SD) sequence. For C-terminal tagging, the donor contained: (a) the SA sequence; (b) the last exon coding sequence followed by the fluorescent tag and stop codon; (c) the SV40 3' processing and polyadenylation sequence (Connelly et al., 1988). The ends of donor were sandwiched between inverted sites for the gene targeting sgRNA, ensuring donor excision by SpCas9 (Connelly et al., 1988) (see Supplementary Figures for plasmid designs). The donor sequence was either PCR amplified (Q5 High-Fidelity DNA polymerase, New England Biolabs) or ordered as a gBlock (Integrated DNA Technologies), digested with restriction enzymes (HindIII-HF and XhoI-HF or BamHI-HF, New England Biolabs), gel purified, and cloned into pORANGE containing the corresponding sgRNA.

The targeting vectors were transiently transfected with Lipofectamine 2000 into MCF10A epithelial cells or HeLa cells together with pCE-mp53DD, an episomal plasmid encoding a dominant-negative mutant of TP53, to avoid apoptosis due to DNA damage responses (Haapaniemi et al., 2018, Ihry et al., 2018). Fluorescent cells were selected by FACS two weeks after transfection and characterized.

Oligonucleotides for *Cas* gene editing

Name	**Sequence and notes**
Cas sgRNA	BbsI-**TARGET**
Cas gRNA Fw	caccg**ATCAGCGGTGTTCACTCAAG**
Cas gRNA Rv	aaac**CTTGAGTGAACACCGCTGAT**c
Cas mScarlet PCR	**HindIII-TARGET-<u>PAM</u>**-*SPLICE DONOR*-mScarlet
mSc Donor HindIII Fw	ata**aagcttATCAGCGGTGTTCACTCAAG<u>GGG</u>***CTAATCTCCTCTC TTCTCCTCTCTCCAG*gtgagcaagggcgaggcagt
	XhoI-<u>PAM</u>-TARGET-*SPLICE ACCEPTOR*-mScarlet
mSc Donor XhoI Rv	ata**ctcgag<u>CCC</u>CTTGAGTGAACACCGCTGAT***AACCAATACTTAC* cttgtacagctcgtccatgcc
Cas Genomic PCR	
a	CACCTCTACATTCTAGCCTGGG

b	GAACCTGCAACCCAAAACAC
c	GCCCCGTAATGCAGAAGAAG
d	GCATGAACTCCTTGATCACTGC
Cas cDNA PCR	
a	TCGGAGCCCCGAGGGCACGCG
b	CACGATGCCCTGGCGCCCATG
c	CCGCGGCACCAACTTCCCTCC
d	CGGGGATGTCGGCGGGGTGCT

Oligonucleotides and gBlocks for *Crk* gene editing

Name	Sequence and notes
Crk sgRNA	BbsI-**TARGET**
Crk gRNA Fw	CACCG**CCCTGCGGCTGGACTTACGT**
Crk gRNA Rv	AAAC**ACGTAAGTCCAGCCGCAGGG**C
Crk Genomic PCR	
a	TGACCCATACAGTGACTTCAGG
b	TTATGCATCTGGGCTTGTACTG
c	GAGCAAAGACCCCAACGAGAA
d	GCTGAACTTGTGGCCGTTTAC
Crk cDNA PCR	
a’	CTGATTGGAGGTAACCAGGAG
b’	GCAGATGAACTTCAGGGTCAG
Crk^{mGL} gBlock (Donor)	**HindIII-PAM-TARGET**-*SPLICE ACCEPTOR*-3’ORF-*GGGS-mGL-stop*-spacer-*SV40polyA*-**PAM-TARGET-BamHI**
	agcata**aagcttCCAACGTAAGTCCAGCCGCAGGG***CTAATCTCCTCTCTTCTCCTCTCTCCAG*GTCGGTGAGCTGGTAAAGGTTACGAAGATTAATGTGAGTGGTCAGTGGGAAGGGGAGTGTAATGGCAAACGAGGTCACTTCCCATTCACACATGTCCGTCTGCTGGATCAACAGAATCCCGATGAGGACTTCAGC*ggcgctagcatggtgagcaagggcgaggagctgttcaccggggtggtgcccatcctggtcgagctgg*

	*acggcgacgtaaacggccacaagttcagcgtgtccggcgagggcgagggcgatgccacc tacggcaagctgaccctgaagttcatctgcaccaccggcaagctgcccgtgccctggccca ccctcgtgaccaccctgacctacggcgtgcagtgcttcagccgctaccccgaccacatgaa gcagcacgacttcttcaagtccgccatgcccgaaggctacgtccaggagcgcaccatcttct tcaaggacgacggcaactacaagacccgcgccgaggtgaagttcgagggcgacaccctg gtgaaccgcatcgagctgaagggcatcgacttcaaggaggacggcaacatcctggggca caagctggagtacaactacaacagccacaacgtctatatcatggccgacaagcagaaga acggcatcaaggtgaacttcaagatccgccacaacatcgaggacggcagcgtgcagctc gccgaccactaccagcagaacacccccatcggcgacggccccgtgctgctgcccgacaa ccactacctgagcacccagtccgccctgagcaaagaccccaacgagaagcgcgatcaca tggtcctgctggagttcgtgaccgccgccgggatcactctcggcatggacgagctgtacaag taa*agcgctccatggccc*AACTTGTTTATTGCAGCTTATAATGGTTACAA ATAAAGCAATAGCATCACAAATTTCACAAATAAAGCATTTTTTTC ACTGCATTCTAGTTGTGGTTTGTCCAAACTCATCAATGTATCTT ATCATGTCTGGATCTC***CCA*AACGTAAGTCCAGCCGCAGGG ggatcc**tatgca

Oligonucleotides and gBlocks for *ITGB1* gene editing

Name	Sequence and notes
ITGB1 sgRNA	BbsI-**TARGET**
ITGB1 gRNA Fw	CACCG**GCGCCTTCTGTTCACGATAA**
ITGB1 gRNA Rv	AAAC**TTATCGTGAACAGAAGGCG**C
ITGB1 Genomic PCR	
a	AGTAACTTCCGTAGGAGACCCC
b	CATTCTTGAGTCCTTCCTCCAC
c	AACGGCATCAAGGTGAACTTC
d	GTAGGTCAGGGTGGTCACGAG
ITGB1 cDNA PCR	
a’	GTGTGGTTGCTGGAATTGTTC
b’	GTAGGTCAGGGTGGTCACGAG

ITGB1^{GFP} gBlock (Donor)	**HindIII-PAM-TARGET-***SPLICE ACCEPTOR*-3'ORF-*linker-GFP-stop*-spacer-*SV40polyA*-**PAM-TARGET-BamHI**
	agcata**aagcttCCTTTATCGTGAACAGAAGGCGC***CTAATCTCCTCTCTTCTCCTCTCTCCAG*GGTGAAAATCCTATTTATAAGAGTGCCGTAACAACTGTGGTCAATCCGAAGTATGAGGGAAA*Aggagggggggggcccggaggcgggggggaggcgggggatccaccggtcgccaccatggtgagcaagggcgaggagctgttcaccggggtggtgcccatcctggtcgagctggacggcgacgtaaacggccacaagttcagcgtgtccggcgagggcgagggcgatgccacctacggcaagctgaccctgaagttcatctgcaccaccggcaagctgcccgtgccctggcccacccctcgtgaccaccctgacctacggcgtgcagtgcttcagccgctaccccgaccacatgaagcagcacgacttcttcaagtccgccatgcccgaaggctacgtccaggagcgcaccatcttcttcaaggacgacggcaactacaagacccgcgccgaggtgaagttcgagggcgacaccctggtgaaccgcatcgagctgaagggcatcgacttcaaggaggacggcaacatcctggggcacaagctggagtacaactacaacagccacaacgtctatatcatggccgacaagcagaagaacggcatcaaggtgaacttcaagatccgccacaacatcgaggacggcagcgtgcagctcgccgaccactaccagcagaacacccccatcggcgacggccccgtgctgctgcccgacaaccactacctgagcacccagtccgccctgagcaaagaccccaacgagaagcgcgatcacatggtcctgctggagttcgtgaccgccgccgggatcactctcggcatggacgagctgtacaagtaa*agcgct*CCATGGCCCAACTTGTTTATTGCAGCTTATAATGGTTACAAATAAAGCAATAGCATCACAAATTTCACAAATAAAGCATTTTTTTCACTGCATTCTAGTTGTGGTTTGTCCAAACTCATCAATGTATCTTATCATGTCTGGATCTC**CCTTTATCGTGAACAGAAGGCGC ggatcc**tatgca

Cell lines, transfection and infection

MCF10A cells were originally obtained from Dr. J. Brugge (Harvard Medical School) and confirmed by STR profiling. Cells were cultured in DMEM/F12 growth media (Thermo Fisher Scientific) supplemented with 5% horse serum, (Thermo Fisher Scientific), 10 μg/ml insulin (Thermo Fisher Scientific), 0.1 μg/ml cholera toxin (EMD Millipore), 0.5 μg/ml hydrocortisone

(Sigma-Aldrich), and 20 ng/ml EGF (Thermo Fisher Scientific) and passaged using trypsin/EDTA or Accutase (Sigma-Aldrich A6964). For experiments, cells were detached with Accutase and resuspended in assay media (DMEM/F12, 2% horse serum, 0.1 μg/ml cholera toxin, 10 μg/ml insulin, 0.5 μg/ml hydrocortisone, and 0 ng/ml EGF).

HeLa cells were initially obtained from ATCC and confirmed by STR DNA profiling. Cells were cultured in DMEM supplemented with 10% FBS and penicillin/streptomycin (both 100U/ml) and passaged with trypsin/EDTA. For experiments, cells were detached using Accutase and resuspended in DMEM without serum.

Retro- and lentiviruses were generated by transfecting 293FT cells with viral vector, pMD2.G and psPAX2 in 2:1:2 ratio with PolyJet transfection reagent (SignaGen Laboratories). Media were harvested two days later and added to recipient cells with 1 μg/ml polybrene (Sigma) for 8-16 hours. Expressing cells were selected using 1 μg/ml puromycin or FACS, depending on the vector.

Antibodies

Following antibodies were used: mouse anti-Cas (610271) (BD Biosciences); rabbit-phospho-Y410Cas (4011S) and phospho-Y249Cas (4014S) (Cell Signaling Technology); mouse anti-vinculin (V9131, Sigma-Aldrich); sheep anti-paxillin (AF4259, R and D Systems); rabbit anti-pY31 paxillin (44-720G, Biosource); rat anti-integrin-β1-activated (9EG7, 553715) and mouse anti-paxillin (610051) (BD Biosciences); rabbit anti-Talin1 (A14168-1-AP), rabbit-anti Kindlin2 (11453-1-AP) and mouse anti-FAK (66258-1-Ig) (Proteintech); mouse anti-integrin β1 (12G10, MAB2247) (Millipore); rat anti-integrin-β1-inactive (AIIB2), mouse anti-integrin α5β1 (P8D4) and mouse anti-integrin α2β1 (P1E6) (Developmental Studies Hybridoma Bank); AlexaFluor 488 goat anti-rabbit IgG (H+L), AlexaFluor 488 goat anti-mouse IgG (H+L), AlexaFluor 647 goat anti-mouse IgG (H+L), AlexaFluor 647 goat anti-sheep IgG (H+L) and AlexaFluor 633 goat anti-rat IgG (H+L) (Invitrogen); IRDye 680RD goat anti-mouse and IRDye 800CW goat anti-rabbit (LI-COR).

Inhibitors

Inhibitor	Source	Concentration
DPI	EMD Millipore, Cat: 300260-10MG	10 μM
eCF506	Cayman Chemical, Cat: 19959	100 nM
EHT1864	ApexBio, Cat: B5487	10 μM
MLN4924	Fisher, Cat: 50161353	5 μM

siRNA transfection

Cells were suspended in growth media and added to dishes with 50 pmol pooled siRNA and RNAiMAX (Invitrogen) as per the manufacturer's instructions. Transfection was repeated two days later and cells analyzed after a further two days.

Negative control siRNA	Qiagen, Cat: 1027280	AAT TCT CCG AAC GTG TCA CGT
siFyn	Dharmacon, Cat: L-003140-00-0005	J-003140-11: CGG AUU GGC CCG AUU GAU A J-003140-12: GGA CUC AUA UGC AAG AUU G J-003140-13: GAA GCC CGC UCC UUG ACA A J-003140-14: GGA GAG ACA GGU UAC AUU C
siCrk	Dharmacon, Cat: M-010503-03-0005	D-010503-02: GGA GAC AUC UUG AGA AUC C D-010503-03: UCC CUU ACG UCG AGA AGU A D-010503-04: GGA CAG CGA AGG CAA GAG A D-010503-19: GGG ACU AUG UGC UCA GCG U
siCrkL	Dharmacon, Cat: M-012023-02-0005	D-012023-01: CCG AAG ACC UGC CCU UUA A D-012023-02: GAA GAU AAC CUG GAA UAU G D-012023-05: AAU AGG AAU UCC AAC AGU U D-012023-18: AGU AAA ACU UAA CGG ACU U
siSOCS6	Qiagen, Cat: GS9306	SI03068359: CAG CTG CGA TAT CAA CGG TGA SI00061383: TAG AAT CGT GAA TTG ACA TAA SI00061376: CGG GTA CAA ATT GGC ATA ACA SI00061369: TTG ATC TAA TTG AGC ATT CAA
siYes1	Qiagen, Cat: GS7525	SI02223942: GAG GCT CCT GCT TAT TTA TAA SI02223935: CCA GCC TAC ATT CAC TTC TAA SI00302218: AAT CCC TCC ATG AAT TGA TGA

		SI02635206: AAG TAT AAT GCA GTA CAT TAA
siBCAR1 (Cas)	Qiagen, Cat: GS9564	SI02757741: AAG CAG TTT GAA CGA CTG GAA SI02757734: CTG GAT GGA GGA CTA TGA CTA SI04438280: CCA GGA ATC TGT ATA TAT TTA SI04438273: CAA CCT GAC CAC ACT GAC CAA
siSrc	Qiagen, Cat: GS6714	SI02664151: CTC CAT GTG CGT CCA TAT TTA SI02223928: CGG CTT GTG GGT GAT GTT TGA SI02223921: AAG CAG TGC CTG CCT ATC AAA SI03041605: ACG GCG CGG CAA GGT GCC AAA
siVinculin	Dharmacon, Cat: L-009288-00-0005	J-009288-05: UGA GAU AAU UCG UGU GUU A J-009288-06: GAG CGA AUC CCA ACC AUA A J-009288-07: GCC AAG CAG UGC ACA GAU A J-009288-08: CAG CAU UUA UUA AGG UUG A
siPTK2 (FAK)	Dharmacon, Cat: L-003164-00-0005	J-003164-13: GCG AUU AUA UGU UAG AGA U J-003164-14: GGG CAU CAU UCA GAA GAU A J-003164-15: UAG UAC AGC UCU UGC AUA U J-003164-16: GGA CAU UAU UGG CCA CUG U
siPaxillin	Dharmacon, Cat: L-005163-00-005	J-005163-05: CAA CUG GAA ACC ACA CAU A J-005163-06: GGA CGU GGC ACC CUG AAC A J-005163-07: CCA AAC GGC CUG UGU UCU U J-005163-08: UGA CGA AAG AGA AGC CUA A
siFERMT2 (Kindlin2)	Dharmacon, Cat: L-012753-00-0005	J-012753-05: GCC CAG GAC UGU AUA GUA A J-012753-06: CUA CAU AUU UCU CUC AAC A J-012753-07: GAA CUG AGU GUC CAU GUG A J-012753-08: AAU GAA AUC UGG CUU CGU U
siTalin1	Dharmacon, Cat: L-012949-00-005	J-012949-05: GAA GAU GGU UGG CGG CAU U J-012949-06: GUA GAG GAC CUG ACA ACA A J-012949-07: UCA AUC AGC UCA UCA CUA U J-012949-08: GAG AUG AGG AGU CUA CUA U

Cell lysis and immunoblotting

Cells were harvested after 30 min of attachment. Cells were washed three times with cold phosphate-buffer saline (PBS) followed by lysis in RIPA buffer (1% Triton X-100, 1% sodium

deoxycholate, 0.1% SDS, 20 mM Tris-HCl pH 7.4, 150 mM NaCl, 5 mM EGTA) with freshly added protease and phosphatase inhibitors (10 µg/mL Aprotinin, 1 mM PMSF, 1 mM sodium vanadate) on ice. The lysates were collected after 30 min of incubation on ice and centrifuged at 12,000 rpm for 10 min at 4 °C. Supernatants were collected and adjusted to equal protein concentration using the Pierce BCA protein assay kit.

Lysates were adjusted to SDS sample buffer, heated at 95°C, and resolved on SDS-PAGE using 15% polyacrylamide/0.133% bis-acrylamide or 12.5% acrylamide/0.1% bis-acrylamide gels, and transferred on to nitrocellulose membrane. Blocking was performed in Odyssey blocking buffer (LI-COR Biosciences) supplemented with 5% BSA for 30 min. After blocking, membrane was probed with the primary antibody overnight, washed in Tris-buffered saline (TBS) 0.1% Tween 20, followed by incubation for 45 min with IRDye 800CW goat anti-rabbit or 680RD goat anti-mouse conjugated secondary antibodies. Images were collected using the Odyssey Infrared Imaging System (LI-COR Biosciences) and quantified using ImageJ.

Cell spreading and migration assays

Cells were treated with siRNA using the double transfection method as described above. Cells were starved overnight in assay media (MCF10A) or DME (HeLa), then detached with Accutase and resuspended in assay media or DME. Cells were incubated for 60 min in 5% CO_2 at 37°C in suspension before adding to glass-bottom dishes (FluoroDish, FD35-100, World Precision Instruments) or 12-mm diameter coverslips (Fisherbrand 1254580) that had been previously coated with 50 µg/ml collagen-I (Advance Biomatrix, #5056) or 5 µg/ml fibronectin (Sigma, #F1141) for at least 3 hr at 37°C and washed with PBS. Pharmacological agents were added just before seeding cells for imaging.

Live-imaging

Dual-color imaging of live cells was performed for a 30-min time period, either immediately after plating the cells, to record attachment and spreading, or approximately 24 hr after plating, to record spontaneous lamellipodia formation. Images were recorded in 4-5 fields of view on a fully automated TIRF microscope (Nikon Ti, 100x/1.49 CFI Apo TIRF oil immersion objective) equipped with Perfect Focus, motorized x-y stage, fast piezo z stage, stage-top incubator with

temperature and CO_2 control, and Andor iXon X3 EMCCD camera with 512 x 512-pixel chip (16 micron pixels). The images were acquired using Nikon NIS Elements software and processed using ImageJ. Frame rate varied between 15 and 20 s depending on the number of fields of view recorded. Slight drift in the dual color time lapse images was corrected using ImageJ registration tool Image Stabilizer.

Cell migration was imaged once every 15 min for 12 hr using phase-contrast microscopy on an IncuCyte S3 and analyzed using ImageJ.

Immunofluorescence

MCF10A Cas^{mSc} cells, either expressing YFP-vinculin or not, were plated on glass-bottom dishes or coverslips and allowed to attach for 30 min before fixation with 4% paraformaldehyde in PBS for 15 min. Cells were permeabilized with 0.1% Triton X-100 in PBS for 5 min, and blocked for an hour in 5% normal goat serum, 2% BSA in PBS, all at room temperature. The cells were incubated with different combinations of primary antibodies (1:200 dilution) for either 2-3 hours at room temperature or overnight at 4 °C, then washed gently three times. Alexa Fluor-conjugated secondary antibodies were added at 1:200 dilution for 1 hr at room temperature. Alexa Fluor 488 or 647-conjugated phalloidin was used for F-actin. Glass-bottom dishes were left in PBS for TIRF microscopy as above. Coverslips were mounted in ProLong Gold (Invitrogen) for confocal microscopy.

Confocal microscopy

Fixed, immunostained coverslips were imaged on the Dragonfly 200 High-speed Spinning disk confocal imaging platform (Andor Technology Ltd.) on a Leica DMi8 microscope stand equipped with iXon EMCCD and sCMOS Zyla camera. The images on Dragonfly were acquired on 100x/1.4 oil immersion objective by using Fusion Version 2.3.0.36 (Oxford Instruments) software together with Imaris simultaneous deconvolution. The most ventral image was used for quantification.

Immunofluorescence quantification

Macros were written in ImageJ for uniform image processing and analysis. Backgrounds were subtracted and intensities adjusted equally across each image set.

For analysis of the spatial distribution of the proteins and phosphoproteins within Cas/vinculin clusters, a line (5x25-pixels width x length, 0.16 micron/pixel) was plotted along the major axis of a Cas^{mSc} cluster, starting from the outer edge and moving inwards. The intensity profile for each antibody along this line was quantified in ImageJ and aligned using Cas^{mSc} as a reference point. The mean normalized intensity profile for each antibody was then calculated across 20-25 regions from several cells. A heat map for the mean intensity profile of the normalized value was generated using GraphPad Prism.

To analyze the number and intensity of clusters containing either Cas or vinculin, or both, images were first spit into individual channels and then summed using the 'Image calculator' command in ImageJ. This summed image was used to generate a binary image mask by applying the manual threshold through Yen method. The number, areas, and median intensity of each channel in regions of interest ≥20 pixels (0.52 μm^2) was quantified for each cell analyzed. Cell area was quantified either manually by drawing around the cell or from a binary mask created by thresholding through the Triangle method, setting minimum size as 50 pixels.

Quantification of cluster kinetics from two-color TIRF videos

TIRF image datasets were exported as two-channel time-series hyperstacks in TIF format. Quantification of the time shift between red (Cas^{mSc}) and green (YFP-VCL, β1-EctopH, $ITGB1^{GFP}$ or Crk^{mGL}) cluster formation was performed in MATLAB (R2021b). The pipeline involves the following steps: drift correction, image preprocessing and denoising, focal adhesion segmentation and tracking, intensities extraction and normalization, and signal analysis.

Drifts between timeframes were corrected by registering the image of one frame to the image of the previous frame using a translation transformation. Drift corrected timeseries were then denoised with a median filter and their background was equalized with a top-hat transform. Clusters were segmented separately in each channel at each timeframe by intensity thresholding and size filtering. Threshold values were arbitrarily defined as a quarter of the intensity value of

the 50th brightest pixel of the dataset for each channel, and the union of the binary masks of the two channels with an area greater than 20 pixels (0.52 μm^2) was used to define clusters. Clusters were tracked over time by creating a 3D stack (XYT) and by computing the resulting connected components. Only clusters tracked in 3 or more frames (≥40 s) were quantified. For each tracked cluster, the average mean intensity of each channel over time was extracted by first measuring the mean intensity within the mask at each timeframe from time zero to the end, resulting in a number of intensity traces equal to the number of timeframes where the cluster was tracked.

To calculate the time shift between the red and green channel intensity profiles for each tracked cluster, average mean intensity traces were rescaled to the [0 1] value range, and after smoothing the signal by applying a moving average filter, the time at which the rescaled intensity reaches 0.5 ($t_{1/2}$) was interpolated. The time shift was finally calculated by subtracting red (Cas) $t_{1/2}$ from green (vinculin, integrin or Crk) $t_{1/2}$.

Adhesome isolation

Adhesome samples were isolated as described with minor modifications (Schiefermeier et al., 2014). MCF10A cells were detached from near-confluent 5-cm plates, resuspended in assay media, incubated in suspension for 30 min, then re-seeded onto an equal number of 5-cm plates that had been precoated with 50 μg/ml collagen. After one hour at 37°C, one dish was washed and lysed in 400 μl RIPA buffer to provide a sample of total protein (T) and the other dishes were washed gently with room temperature PBS and incubated with 2 ml freshly diluted 0.5 mM dithiobis(succinimidyl propionate) (DSP, EMD Millipore 322133) 0.05 mM (1,4-di [3'-(2'-pyridyldithio)propionamido] butane) (DPDPB, Sigma 16646) in PBS for 5 min at room temperature. Cross-linking was terminated by washing twice with 50 mM Tris 140 mM NaCl pH7.4 before transferring to ice. 400 μl RIPA buffer was added and the plates were rocked at 4°C for 1 hr. Supernatants (S) were collected in a 2-ml microtube (Axygen MCT-200-L-C). The plates were washed twice with PBS, drained, and 400 μl RIPA buffer added. 2-Mercaptoethanol was added to 2% concentration to all samples, and all microtubes and dishes were sealed and incubated at 50°C for 1 hr. After cooling to room temperature, the dish was scraped and the adhesome (A) fraction was transferred to a 2-ml microtube. Total, supernatant and adhesome fractions were sonicated (10 s, microtip) to shear DNA and the proteins were precipitated by

adding 1.6 ml acetone and placing at -20°C for 1 hr. After centrifugation (10 min, 14,000 rpm), pellets were drained, dried in a stream of air, and incubated with 25 μl 5x concentrated SDS sample buffer at 95°C for 5 min, then 100 μl RIPA buffer was added to all tubes. Samples were centrifuged and equal volumes analyzed by SDS PAGE, typically on 10% acrylamide/0.13% bisacrylamide gels, followed by Western blotting. The procedure was scaled up as needed to run replicate blots for probing with different antibody combinations. On occasion, dilutions of the T sample were loaded to estimate detection sensitivity.

Ratiometric FRET imaging

Rac1-2G reporter was expressed in MCF10A cells by lentiviral transduction. After siRNA or inhibitor treatment, cells were allowed to attach to collagen for 30 min then fixed and mounted. Coverslips were imaged on a Leica SP8 confocal microscope using Leica HCX Plan Apo 63X/ 1.40 oil immersion objective. Excitation and emission wavelengths as follows: donor (mTFP1) excitation 440 nm, emission 450-510 nm: FRET excitation 440 nm, emission 515-600 nm; acceptor (mVenus) excitation 514 nm, emission 515-600 nm. All channels were collected on the HyD detectors. Images were processed with the Lightening deconvolution (Leica LASX software) and FRET ratio in the most ventral plane quantified using ImageJ as described (Kardash et al., 2011).

Statistics

Distributions were analyzed using GraphPad Prism. Median and 95% confidence intervals were calculated for non-normal distributions. Data from multiple cells or biological replicates were assumed to follow normal distributions allowing calculation of mean and standard deviation (SD), or standard error of the mean (SEM) in cases where data from multiple cells in biologically independent experiments were combined. Comparisons between control and experimental populations were made using the non-parametric Mann Whitney U-test except where noted. In some experiments, a single control was compared with multiple experimental conditions. If the experimental conditions tested alternative hypotheses, we used the non-parametric Kruskal-Wallis ANOVA followed by Dunn’s multiple comparison test.

Acknowledgements

We are very grateful to Lena Schroeder, Peng Guo and Jin Meng for instruction and use of the Cellular Imaging Shared Resource and Luna Yu for computational assistance. We thank Dorus Gadella, Harold MacGillavry, Shinya Yamanaka, Olivier Pertz, Gregory Petsko and Didier Trono for Addgene plasmids and David Calderwood and Susumu Antoku for additional constructs. Reinhard Faessler provided a detailed protocol for adhesome isolation. We are very grateful for helpful discussions with Matt Berginski and Matthew Kutys. Dayoung Kim, Jihong Bai, Cecilia Moens, Susan Parkhurst and other colleagues provided useful feedback during development of the project. This research was supported by institutional funds from Fred Hutch and National Institutes of Health grant R01 GM109463 from the US Public Health Service. The Cellular Imaging Shared Resource of the Fred Hutch/University of Washington Cancer Consortium is supported by P30 CA015704.

Alfandari D, Cousin H, Gaultier A, Hoffstrom BG, DeSimone DW. 2003. Integrin alpha5beta1 supports the migration of Xenopus cranial neural crest on fibronectin. *Dev Biol* **260**:449-64. doi: 10.1016/s0012-1606(03)00277-x.

Anthis NJ, Wegener KL, Critchley DR, Campbell ID. 2010. Structural diversity in integrin/talin interactions. *Structure* **18**:1654-66. doi: 10.1016/j.str.2010.09.018.

Arias-Salgado EG, Lizano S, Sarkar S, Brugge JS, Ginsberg MH, Shattil SJ. 2003. Src kinase activation by direct interaction with the integrin beta cytoplasmic domain. *Proc Natl Acad Sci U S A* **100**:13298-302. doi: 10.1073/pnas.2336149100.

Arthur WT, Quilliam LA, Cooper JA. 2004. Rap1 promotes cell spreading by localizing Rac guanine nucleotide exchange factors. *J Cell Biol* **167**:111-22. doi: 10.1083/jcb.200404068.

Bachir AI, Zareno J, Moissoglu K, Plow EF, Gratton E, Horwitz AR. 2014. Integrin-associated complexes form hierarchically with variable stoichiometry in nascent adhesions. *Curr Biol* **24**:1845-53. doi: 10.1016/j.cub.2014.07.011.

Bazzoni G, Shih DT, Buck CA, Hemler ME. 1995. Monoclonal antibody 9EG7 defines a novel beta 1 integrin epitope induced by soluble ligand and manganese, but inhibited by calcium. *J Biol Chem* **270**:25570-7. doi: 10.1074/jbc.270.43.25570.

Beckham Y, Vasquez RJ, Stricker J, Sayegh K, Campillo C, Gardel ML. 2014. Arp2/3 inhibition induces amoeboid-like protrusions in MCF10A epithelial cells by reduced cytoskeletal-membrane coupling and focal adhesion assembly. *PLoS One* **9**:e100943. doi: 10.1371/journal.pone.0100943.

Bockholt SM, Burridge K. 1995. An examination of focal adhesion formation and tyrosine phosphorylation in fibroblasts isolated from src-, fyn-, and yes- mice. *Cell Adhes Commun* **3**:91-100. doi: 10.3109/15419069509081279.

Brandman O, Meyer T. 2008. Feedback loops shape cellular signals in space and time. *Science* **322**:390-5. doi: 10.1126/science.1160617.

Buensuceso C, de Virgilio M, Shattil SJ. 2003. Detection of integrin alpha IIbbeta 3 clustering in living cells. *J Biol Chem* **278**:15217-24. doi: 10.1074/jbc.M213234200.

Burridge K, Chrzanowska-Wodnicka M. 1996. Focal adhesions, contractility, and signaling. *Annu Rev Cell Dev Biol* **12**:463-518. doi: 10.1146/annurev.cellbio.12.1.463.

Burridge K, Turner CE, Romer LH. 1992. Tyrosine phosphorylation of paxillin and pp125FAK accompanies cell adhesion to extracellular matrix: a role in cytoskeletal assembly. *J Cell Biol* **119**:893-903.

Cabodi S, del Pilar Camacho-Leal M, Di Stefano P, Defilippi P. 2010. Integrin signalling adaptors: not only figurants in the cancer story. *Nat Rev Cancer* **10**:858-70. doi: 10.1038/nrc2967.

Campbell BC, Nabel EM, Murdock MH, Lao-Peregrin C, Tsoulfas P, Blackmore MG, Lee FS, Liston C, Morishita H, Petsko GA. 2020. mGreenLantern: a bright monomeric fluorescent protein with rapid expression and cell filling properties for neuronal imaging. *Proc Natl Acad Sci U S A* **117**:30710-30721. doi: 10.1073/pnas.2000942117.

Carter WG, Wayner EA, Bouchard TS, Kaur P. 1990. The role of integrins alpha 2 beta 1 and alpha 3 beta 1 in cell-cell and cell-substrate adhesion of human epidermal cells. *J Cell Biol* **110**:1387-404. doi: 10.1083/jcb.110.4.1387.

Case LB, De Pasquale M, Henry L, Rosen MK. 2022. Synergistic phase separation of two pathways promotes integrin clustering and nascent adhesion formation. *Elife* **11**. doi: 10.7554/eLife.72588.

Chodniewicz D, Klemke RL. 2004. Regulation of integrin-mediated cellular responses through assembly of a CAS/Crk scaffold. *Biochim Biophys Acta* **1692**:63-76. doi: 10.1016/j.bbamcr.2004.03.006.

Choi CK, Vicente-Manzanares M, Zareno J, Whitmore LA, Mogilner A, Horwitz AR. 2008. Actin and alpha-actinin orchestrate the assembly and maturation of nascent adhesions in a myosin II motor-independent manner. *Nat Cell Biol* **10**:1039-50. doi: 10.1038/ncb1763.

Connelly S, Manley JL. 1988. A functional mRNA polyadenylation signal is required for transcription termination by RNA polymerase II. *Genes Dev* **2**:440-52. doi: 10.1101/gad.2.4.440.

Davidson LA, Hoffstrom BG, Keller R, DeSimone DW. 2002. Mesendoderm extension and mantle closure in Xenopus laevis gastrulation: combined roles for integrin alpha(5)beta(1), fibronectin, and tissue geometry. *Dev Biol* **242**:109-29. doi: 10.1006/dbio.2002.0537.

Debnath J, Brugge JS. 2005. Modelling glandular epithelial cancers in three-dimensional cultures. *Nat Rev Cancer* **5**:675-88.

Donato DM, Ryzhova LM, Meenderink LM, Kaverina I, Hanks SK. 2010. Dynamics and mechanism of p130Cas localization to focal adhesions. *J Biol Chem* **285**:20769-79. doi: 10.1074/jbc.M109.091207.

Eliceiri BP, Puente XS, Hood JD, Stupack DG, Schlaepfer DD, Huang XZ, Sheppard D, Cheresh DA. 2002. Src-mediated coupling of focal adhesion kinase to integrin alpha(v)beta5 in vascular endothelial growth factor signaling. *J Cell Biol* **157**:149-60. doi: 10.1083/jcb.200109079.

Felsenfeld DP, Schwartzberg PL, Venegas A, Tse R, Sheetz MP. 1999. Selective regulation of integrin--cytoskeleton interactions by the tyrosine kinase Src. *Nat Cell Biol* **1**:200-6. doi: 10.1038/12021.

Fraser C, Dawson JC, Dowling R, Houston DR, Weiss JT, Munro AF, Muir M, Harrington L, Webster SP, Frame MC, Brunton VG, Patton EE, Carragher NO, Unciti-Broceta A. 2016. Rapid Discovery and Structure-Activity Relationships of Pyrazolopyrimidines That Potently Suppress Breast Cancer Cell Growth via SRC Kinase Inhibition with Exceptional Selectivity over ABL Kinase. *J Med Chem* **59**:4697-710. doi: 10.1021/acs.jmedchem.6b00065.

Fritz RD, Menshykau D, Martin K, Reimann A, Pontelli V, Pertz O. 2015. SrGAP2-Dependent Integration of Membrane Geometry and Slit-Robo-Repulsive Cues Regulates Fibroblast Contact Inhibition of Locomotion. *Dev Cell* **35**:78-92. doi: 10.1016/j.devcel.2015.09.002.

Gailit J, Ruoslahti E. 1988. Regulation of the fibronectin receptor affinity by divalent cations. *J Biol Chem* **263**:12927-32.

Garton AJ, Flint AJ, Tonks NK. 1996. Identification of p130(cas) as a substrate for the cytosolic protein tyrosine phosphatase PTP-PEST. *Mol Cell Biol* **16**:6408-18. doi: 10.1128/MCB.16.11.6408.

Giannoni E, Buricchi F, Raugei G, Ramponi G, Chiarugi P. 2005. Intracellular reactive oxygen species activate Src tyrosine kinase during cell adhesion and anchorage-dependent cell growth. *Mol Cell Biol* **25**:6391-403. doi: 10.1128/MCB.25.15.6391-6403.2005.

Gotoh T, Hattori S, Nakamura S, Kitayama H, Noda M, Takai Y, Kaibuchi K, Matsui H, Hatase O, Takahashi H, et al. 1995. Identification of Rap1 as a target for the Crk SH3 domain-binding guanine nucleotide-releasing factor C3G. *Mol Cell Biol* **15**:6746-53. doi: 10.1128/MCB.15.12.6746.

Haapaniemi E, Botla S, Persson J, Schmierer B, Taipale J. 2018. CRISPR-Cas9 genome editing induces a p53-mediated DNA damage response. *Nat Med* **24**:927-930. doi: 10.1038/s41591-018-0049-z.

Han SJ, Azarova EV, Whitewood AJ, Bachir A, Guttierrez E, Groisman A, Horwitz AR, Goult BT, Dean KM, Danuser G. 2021. Pre-complexation of talin and vinculin without tension is required for efficient nascent adhesion maturation. *Elife* **10**. doi: 10.7554/eLife.66151.

Harte MT, Hildebrand JD, Burnham MR, Bouton AH, Parsons JT. 1996. p130Cas, a substrate associated with v-Src and v-Crk, localizes to focal adhesions and binds to focal adhesion kinase. *J Biol Chem* **271**:13649-55. doi: 10.1074/jbc.271.23.13649.

Hasegawa H, Kiyokawa E, Tanaka S, Nagashima K, Gotoh N, Shibuya M, Kurata T, Matsuda M. 1996. DOCK180, a major CRK-binding protein, alters cell morphology upon translocation to the cell membrane. *Mol Cell Biol* **16**:1770-6. doi: 10.1128/MCB.16.4.1770.

Henning Stumpf B, Ambriovic-Ristov A, Radenovic A, Smith AS. 2020. Recent advances and prospects in the research of nascent adhesions. *Front Physiol* **11**:574371. doi: 10.3389/fphys.2020.574371.

Honda H, Nakamoto T, Sakai R, Hirai H. 1999. p130(Cas), an assembling molecule of actin filaments, promotes cell movement, cell migration, and cell spreading in fibroblasts. *Biochem Biophys Res Commun* **262**:25-30. doi: 10.1006/bbrc.1999.1162.

Honda H, Oda H, Nakamoto T, Honda Z, Sakai R, Suzuki T, Saito T, Nakamura K, Nakao K, Ishikawa T, Katsuki M, Yazaki Y, Hirai H. 1998. Cardiovascular anomaly, impaired actin bundling and resistance to Src-induced transformation in mice lacking p130Cas. *Nat Genet* **19**:361-5. doi: 10.1038/1246.

Horton ER, Byron A, Askari JA, Ng DHJ, Millon-Fremillon A, Robertson J, Koper EJ, Paul NR, Warwood S, Knight D, Humphries JD, Humphries MJ. 2015. Definition of a consensus integrin adhesome and its dynamics during adhesion complex assembly and disassembly. *Nat Cell Biol* **17**:1577-1587. doi: 10.1038/ncb3257.

Huang MM, Lipfert L, Cunningham M, Brugge JS, Ginsberg MH, Shattil SJ. 1993. Adhesive ligand binding to integrin alpha IIb beta 3 stimulates tyrosine phosphorylation of novel protein substrates before phosphorylation of pp125FAK. *J Cell Biol* **122**:473-83.

Huet-Calderwood C, Rivera-Molina F, Iwamoto DV, Kromann EB, Toomre D, Calderwood DA. 2017. Novel ecto-tagged integrins reveal their trafficking in live cells. *Nat Commun* **8**:570. doi: 10.1038/s41467-017-00646-w.

Humphries JD, Byron A, Bass MD, Craig SE, Pinney JW, Knight D, Humphries MJ. 2009. Proteomic analysis of integrin-associated complexes identifies RCC2 as a dual regulator of Rac1 and Arf6. *Sci Signal* **2**:ra51. doi: 10.1126/scisignal.2000396.

Hynes RO. 2002. Integrins: bidirectional, allosteric signaling machines. *Cell* **110**:673-87.

Ihry RJ, Worringer KA, Salick MR, Frias E, Ho D, Theriault K, Kommineni S, Chen J, Sondey M, Ye C, Randhawa R, Kulkarni T, Yang Z, McAllister G, Russ C, Reece-Hoyes J, Forrester W, Hoffman GR, Dolmetsch R, Kaykas A. 2018. p53 inhibits CRISPR-Cas9 engineering in human pluripotent stem cells. *Nat Med* **24**:939-946. doi: 10.1038/s41591-018-0050-6.

Iwamoto DV, Calderwood DA. 2015. Regulation of integrin-mediated adhesions. *Curr Opin Cell Biol* **36**:41-7. doi: 10.1016/j.ceb.2015.06.009.

Janostiak R, Brabek J, Auernheimer V, Tatarova Z, Lautscham LA, Dey T, Gemperle J, Merkel R, Goldmann WH, Fabry B, Rosel D. 2014. CAS directly interacts with vinculin to control mechanosensing and focal adhesion dynamics. *Cell Mol Life Sci* **71**:727-44. doi: 10.1007/s00018-013-1450-x.

Kanchanawong P, Calderwood DA. 2022. Organization, dynamics and mechanoregulation of integrin-mediated cell-ECM adhesions. *Nat Rev Mol Cell Biol*. doi: 10.1038/s41580-022-00531-5.

Kanchanawong P, Shtengel G, Pasapera AM, Ramko EB, Davidson MW, Hess HF, Waterman CM. 2010. Nanoscale architecture of integrin-based cell adhesions. *Nature* **468**:580-4. doi: 10.1038/nature09621.

Kardash E, Bandemer J, Raz E. 2011. Imaging protein activity in live embryos using fluorescence resonance energy transfer biosensors. *Nat Protoc* **6**:1835-46. doi: 10.1038/nprot.2011.395.

Karginov AV, Ding F, Kota P, Dokholyan NV, Hahn KM. 2010. Engineered allosteric activation of kinases in living cells. *Nat Biotechnol* **28**:743-7. doi: 10.1038/nbt.1639.

Klemke RL, Leng J, Molander R, Brooks PC, Vuori K, Cheresh DA. 1998. CAS/Crk coupling serves as a "molecular switch" for induction of cell migration. *Journal of Cell Biology* **140**:961-972. doi: DOI 10.1083/jcb.140.4.961.

Knudsen BS, Feller SM, Hanafusa H. 1994. Four proline-rich sequences of the guanine-nucleotide exchange factor C3G bind with unique specificity to the first Src homology 3 domain of Crk. *J Biol Chem* **269**:32781-7.

Kostic A, Sheetz MP. 2006. Fibronectin rigidity response through Fyn and p130Cas recruitment to the leading edge. *Mol Biol Cell* **17**:2684-95. doi: 10.1091/mbc.e05-12-1161.

Kulak NA, Pichler G, Paron I, Nagaraj N, Mann M. 2014. Minimal, encapsulated proteomic-sample processing applied to copy-number estimation in eukaryotic cells. *Nat Methods* **11**:319-24. doi: 10.1038/nmeth.2834.

Labun K, Montague TG, Krause M, Torres Cleuren YN, Tjeldnes H, Valen E. 2019. CHOPCHOP v3: expanding the CRISPR web toolbox beyond genome editing. *Nucleic Acids Res* **47**:W171-W174. doi: 10.1093/nar/gkz365.

Laukaitis CM, Webb DJ, Donais K, Horwitz AF. 2001. Differential dynamics of alpha 5 integrin, paxillin, and alpha-actinin during formation and disassembly of adhesions in migrating cells. *J Cell Biol* **153**:1427-40. doi: 10.1083/jcb.153.7.1427.

Law DA, Nannizzi-Alaimo L, Phillips DR. 1996. Outside-in integrin signal transduction. Alpha IIb beta 3-(GP IIb IIIa) tyrosine phosphorylation induced by platelet aggregation. *J Biol Chem* **271**:10811-5. doi: 10.1074/jbc.271.18.10811.

Le Coq J, Acebron I, Rodrigo Martin B, Lopez Navajas P, Lietha D. 2022. New insights into FAK structure and function in focal adhesions. *J Cell Sci* **135**. doi: 10.1242/jcs.259089.

Legerstee K, Houtsmuller AB. 2021. A Layered View on Focal Adhesions. *Biology (Basel)* **10**. doi: 10.3390/biology10111189.

Lenter M, Uhlig H, Hamann A, Jeno P, Imhof B, Vestweber D. 1993. A monoclonal antibody against an activation epitope on mouse integrin chain beta 1 blocks adhesion of lymphocytes to the endothelial integrin alpha 6 beta 1. *Proc Natl Acad Sci U S A* **90**:9051-5. doi: 10.1073/pnas.90.19.9051.

Lietha D, Izard T. 2020. Roles of Membrane Domains in Integrin-Mediated Cell Adhesion. *Int J Mol Sci* **21**. doi: 10.3390/ijms21155531.

Lu Z, Mathew S, Chen J, Hadziselimovic A, Palamuttam R, Hudson BG, Fassler R, Pozzi A, Sanders CR, Zent R. 2016. Implications of the differing roles of the beta1 and beta3 transmembrane and cytoplasmic domains for integrin function. *Elife* **5**. doi: 10.7554/eLife.18633.

Ly T, Endo A, Brenes A, Gierlinski M, Afzal V, Pawellek A, Lamond AI. 2018. Proteome-wide analysis of protein abundance and turnover remodelling during oncogenic transformation of human breast epithelial cells. *Wellcome Open Res* **3**:51. doi: 10.12688/wellcomeopenres.14392.1.

Mace PD, Wallez Y, Dobaczewska MK, Lee JJ, Robinson H, Pasquale EB, Riedl SJ. 2011. NSP-Cas protein structures reveal a promiscuous interaction module in cell signaling. *Nat Struct Mol Biol* **18**:1381-7. doi: 10.1038/nsmb.2152.

Machiyama H, Hirata H, Loh XK, Kanchi MM, Fujita H, Tan SH, Kawauchi K, Sawada Y. 2014. Displacement of p130Cas from focal adhesions links actomyosin contraction to cell migration. *J Cell Sci*. doi: 10.1242/jcs.143438.

Mayor R, Etienne-Manneville S. 2016. The front and rear of collective cell migration. *Nat Rev Mol Cell Biol* **17**:97-109. doi: 10.1038/nrm.2015.14.

Meenderink LM, Ryzhova LM, Donato DM, Gochberg DF, Kaverina I, Hanks SK. 2010. P130Cas Src-binding and substrate domains have distinct roles in sustaining focal adhesion disassembly and promoting cell migration. *PLoS One* **5**:e13412. doi: 10.1371/journal.pone.0013412.

Mitra SK, Schlaepfer DD. 2006. Integrin-regulated FAK-Src signaling in normal and cancer cells. *Curr Opin Cell Biol* **18**:516-23. doi: 10.1016/j.ceb.2006.08.011.

Miyamoto S, Teramoto H, Coso OA, Gutkind JS, Burbelo PD, Akiyama SK, Yamada KM. 1995. Integrin function: molecular hierarchies of cytoskeletal and signaling molecules. *J Cell Biol* **131**:791-805. doi: 10.1083/jcb.131.3.791.

Moser M, Legate KR, Zent R, Fassler R. 2009. The tail of integrins, talin, and kindlins. *Science* **324**:895-9. doi: 10.1126/science.1163865.

Nakamoto T, Sakai R, Honda H, Ogawa S, Ueno H, Suzuki T, Aizawa S, Yazaki Y, Hirai H. 1997. Requirements for localization of p130cas to focal adhesions. *Mol Cell Biol* **17**:3884-97. doi: 10.1128/MCB.17.7.3884.

Nimnual AS, Taylor LJ, Bar-Sagi D. 2003. Redox-dependent downregulation of Rho by Rac. *Nat Cell Biol* **5**:236-41. doi: 10.1038/ncb938.

Nobes CD, Hall A. 1995. Rho, rac, and cdc42 GTPases regulate the assembly of multimolecular focal complexes associated with actin stress fibers, lamellipodia, and filopodia. *Cell* **81**:53-62. doi: 10.1016/0092-8674(95)90370-4.

Nojima Y, Morino N, Mimura T, Hamasaki K, Furuya H, Sakai R, Sato T, Tachibana K, Morimoto C, Yazaki Y, Hirai H. 1995. Integrin-mediated cell adhesion promotes tyrosine phosphorylation of p130Cas, a Src homology 3-containing molecule having multiple Src homology 2-binding motifs. *J Biol Chem* **270**:15398-402.

Onesto C, Shutes A, Picard V, Schweighoffer F, Der CJ. 2008. Characterization of EHT 1864, a novel small molecule inhibitor of Rac family small GTPases. *Methods Enzymol* **439**:111-29. doi: 10.1016/S0076-6879(07)00409-0.

Parsons JT, Horwitz AR, Schwartz MA. 2010. Cell adhesion: integrating cytoskeletal dynamics and cellular tension. *Nat Rev Mol Cell Biol* **11**:633-43. doi: 10.1038/nrm2957.

Parsons M, Messent AJ, Humphries JD, Deakin NO, Humphries MJ. 2008. Quantification of integrin receptor agonism by fluorescence lifetime imaging. *J Cell Sci* **121**:265-71. doi: 10.1242/jcs.018440.

Pelham RJ, Jr., Wang Y. 1997. Cell locomotion and focal adhesions are regulated by substrate flexibility. *Proc Natl Acad Sci U S A* **94**:13661-5. doi: 10.1073/pnas.94.25.13661.

Pellicena P, Miller WT. 2001. Processive phosphorylation of p130Cas by Src depends on SH3-polyproline interactions. *J Biol Chem* **276**:28190-6. doi: 10.1074/jbc.M100055200.

Petch LA, Bockholt SM, Bouton A, Parsons JT, Burridge K. 1995. Adhesion-induced tyrosine phosphorylation of the p130 src substrate. *J Cell Sci* **108 (Pt 4)**:1371-9. doi: 10.1242/jcs.108.4.1371.

Polte TR, Hanks SK. 1995. Interaction between focal adhesion kinase and Crk-associated kinase substrate p130cas. *Proc. Natl. Acad. Sci. USA* **92**:10678-10682.

Pratt SJ, Epple H, Ward M, Feng Y, Braga VM, Longmore GD. 2005. The LIM protein Ajuba influences p130Cas localization and Rac1 activity during cell migration. *J Cell Biol* **168**:813-24. doi: 10.1083/jcb.200406083.

Pylayeva Y, Gillen KM, Gerald W, Beggs HE, Reichardt LF, Giancotti FG. 2009. Ras- and PI3K-dependent breast tumorigenesis in mice and humans requires focal adhesion kinase signaling. *J Clin Invest* **119**:252-66. doi: 10.1172/JCI37160.

Reis J, Massari M, Marchese S, Ceccon M, Aalbers FS, Corana F, Valente S, Mai A, Magnani F, Mattevi A. 2020. A closer look into NADPH oxidase inhibitors: Validation and insight into their mechanism of action. *Redox Biol* **32**:101466. doi: 10.1016/j.redox.2020.101466.

Resh MD. 1999. Fatty acylation of proteins: new insights into membrane targeting of myristoylated and palmitoylated proteins. *Biochim Biophys Acta* **1451**:1-16. doi: 10.1016/s0167-4889(99)00075-0.

Robertson J, Jacquemet G, Byron A, Jones MC, Warwood S, Selley JN, Knight D, Humphries JD, Humphries MJ. 2015. Defining the phospho-adhesome through the phosphoproteomic analysis of integrin signalling. *Nat Commun* **6**:6265. doi: 10.1038/ncomms7265.

Rorth P. 2011. Whence directionality: guidance mechanisms in solitary and collective cell migration. *Dev Cell* **20**:9-18. doi: 10.1016/j.devcel.2010.12.014.

Sandilands E, Frame MC. 2008. Endosomal trafficking of Src tyrosine kinase. *Trends Cell Biol* **18**:322-9. doi: 10.1016/j.tcb.2008.05.004.

Schiefermeier N, Scheffler JM, de Araujo ME, Stasyk T, Yordanov T, Ebner HL, Offterdinger M, Munck S, Hess MW, Wickstrom SA, Lange A, Wunderlich W, Fassler R, Teis D, Huber LA. 2014. The late endosomal p14-MP1 (LAMTOR2/3) complex regulates focal adhesion dynamics during cell migration. *J Cell Biol* **205**:525-40. doi: 10.1083/jcb.201310043.

Schiller HB, Friedel CC, Boulegue C, Fassler R. 2011. Quantitative proteomics of the integrin adhesome show a myosin II-dependent recruitment of LIM domain proteins. *EMBO Rep* **12**:259-66. doi: 10.1038/embor.2011.5.

Schoenwaelder SM, Burridge K. 1999. Bidirectional signaling between the cytoskeleton and integrins. *Curr Opin Cell Biol* **11**:274-86. doi: 10.1016/s0955-0674(99)80037-4.

Serebrenik YV, Sansbury SE, Kumar SS, Henao-Mejia J, Shalem O. 2019. Efficient and flexible tagging of endogenous genes by homology-independent intron targeting. *Genome Res* **29**:1322-1328. doi: 10.1101/gr.246413.118.

Smith DJ. 1997. Mini-exon epitope tagging for analysis of the protein coding potential of genomic sequence. *Biotechniques* **23**:116-20. doi: 10.2144/97231st01.

Steenkiste EM, Berndt JD, Pilling C, Simpkins C, Cooper JA. 2021. A Cas-BCAR3 co-regulatory circuit controls lamellipodia dynamics. *Elife* **10**:2021.01.29.428899. doi: 10.7554/eLife.67078.

Stradal TE, Rottner K, Disanza A, Confalonieri S, Innocenti M, Scita G. 2004. Regulation of actin dynamics by WASP and WAVE family proteins. *Trends Cell Biol* **14**:303-11. doi: 10.1016/j.tcb.2004.04.007.

Su Y, Xia W, Li J, Walz T, Humphries MJ, Vestweber D, Cabanas C, Lu C, Springer TA. 2016. Relating conformation to function in integrin alpha5beta1. *Proc Natl Acad Sci U S A* **113**:E3872-81. doi: 10.1073/pnas.1605074113.

Takada Y, Puzon W. 1993. Identification of a regulatory region of integrin beta 1 subunit using activating and inhibiting antibodies. *J Biol Chem* **268**:17597-601.

Takenawa T, Suetsugu S. 2007. The WASP-WAVE protein network: connecting the membrane to the cytoskeleton. *Nat Rev Mol Cell Biol* **8**:37-48. doi: 10.1038/nrm2069.

Tanaka S, Morishita T, Hashimoto Y, Hattori S, Nakamura S, Shibuya M, Matuoka K, Takenawa T, Kurata T, Nagashima K, Matsuda M. 1994. C3G, a guanine nucleotide-releasing protein expressed ubiquitously, binds to the Src homology 3 domains of CRK and GRB2/ASH proteins. *Proc Natl Acad Sci U S A* **91**:3443-7.

Teckchandani A, Cooper JA. 2016. The ubiquitin-proteasome system regulates focal adhesions at the leading edge of migrating cells. *Elife* **5**. doi: 10.7554/eLife.17440.

Teckchandani A, Laszlo GS, Simo S, Shah K, Pilling C, Strait AA, Cooper JA. 2014. Cullin 5 destabilizes Cas to inhibit Src-dependent cell transformation. *J Cell Sci* **127**:509-20. doi: 10.1242/jcs.127829.

Tonks NK. 2005. Redox redux: revisiting PTPs and the control of cell signaling. *Cell* **121**:667-70.

Tuckwell D, Calderwood DA, Green LJ, Humphries MJ. 1995. Integrin alpha 2 I-domain is a binding site for collagens. *J Cell Sci* **108 (Pt 4)**:1629-37. doi: 10.1242/jcs.108.4.1629.

Ushio-Fukai M. 2006. Localizing NADPH oxidase-derived ROS. *Sci STKE* **2006**:re8. doi: 10.1126/stke.3492006re8.

van der Flier S, Brinkman A, Look MP, Kok EM, Meijer-van Gelder ME, Klijn JG, Dorssers LC, Foekens JA. 2000. Bcar1/p130Cas protein and primary breast cancer: prognosis and response to tamoxifen treatment. *J Natl Cancer Inst* **92**:120-7. doi: 10.1093/jnci/92.2.120.

von Wichert G, Haimovich B, Feng GS, Sheetz MP. 2003. Force-dependent integrin-cytoskeleton linkage formation requires downregulation of focal complex dynamics by Shp2. *EMBO J* **22**:5023-35. doi: 10.1093/emboj/cdg492.

Vuori K, Ruoslahti E. 1995. Tyrosine phosphorylation of p130Cas and cortactin accompanies integrin-mediated cell adhesion to extracellular matrix. *J Biol Chem* **270**:22259-62. doi: 10.1074/jbc.270.38.22259.

Wallez Y, Mace PD, Pasquale EB, Riedl SJ. 2012. NSP-CAS protein complexes: emerging sgnaling modules in cancer. *Genes Cancer* **3**:382-93. doi: 10.1177/1947601912460050.

Webb DJ, Donais K, Whitmore LA, Thomas SM, Turner CE, Parsons JT, Horwitz AF. 2004. FAK-Src signalling through paxillin, ERK and MLCK regulates adhesion disassembly. *Nat Cell Biol* **6**:154-61. doi: 10.1038/ncb1094.

Webb DJ, Parsons JT, Horwitz AF. 2002. Adhesion assembly, disassembly and turnover in migrating cells -- over and over and over again. *Nat Cell Biol* **4**:E97-100. doi: 10.1038/ncb0402-e97.

Wendt MK, Smith JA, Schiemann WP. 2009. p130Cas is required for mammary tumor growth and transforming growth factor-beta-mediated metastasis through regulation of Smad2/3 activity. *J Biol Chem* **284**:34145-56. doi: 10.1074/jbc.M109.023614.

Willems J, de Jong APH, Scheefhals N, Mertens E, Catsburg LAE, Poorthuis RB, de Winter F, Verhaagen J, Meye FJ, MacGillavry HD. 2020. ORANGE: A CRISPR/Cas9-based genome editing toolbox for epitope tagging of endogenous proteins in neurons. *PLoS Biol* **18**:e3000665. doi: 10.1371/journal.pbio.3000665.

Wolfenson H, Yang B, Sheetz MP. 2019. Steps in Mechanotransduction Pathways that Control Cell Morphology. *Annu Rev Physiol* **81**:585-605. doi: 10.1146/annurev-physiol-021317-121245.

Yano H, Uchida H, Iwasaki T, Mukai M, Akedo H, Nakamura K, Hashimoto S, Sabe H. 2000. Paxillin alpha and Crk-associated substrate exert opposing effects on cell migration and contact inhibition of growth through tyrosine phosphorylation. *Proc Natl Acad Sci U S A* **97**:9076-81. doi: 10.1073/pnas.97.16.9076.

Zaidel-Bar R, Ballestrem C, Kam Z, Geiger B. 2003. Early molecular events in the assembly of matrix adhesions at the leading edge of migrating cells. *J Cell Sci* **116**:4605-13. doi: 10.1242/jcs.00792.

Zhang C, Miller DJ, Guibao CD, Donato DM, Hanks SK, Zheng JJ. 2017. Structural and functional insights into the interaction between the Cas family scaffolding protein p130Cas and the focal adhesion-associated protein paxillin. *J Biol Chem* **292**:18281-18289. doi: 10.1074/jbc.M117.807271.

Zhang X, Moore SW, Iskratsch T, Sheetz MP. 2014. N-WASP-directed actin polymerization activates Cas phosphorylation and lamellipodium spreading. *J Cell Sci* **127**:1394-405. doi: 10.1242/jcs.134692.

Zhong H, Ceballos CC, Massengill CI, Muniak MA, Ma L, Qin M, Petrie SK, Mao T. 2021. High-fidelity, efficient, and reversible labeling of endogenous proteins using CRISPR-based designer exon insertion. *Elife* **10**. doi: 10.7554/eLife.64911.

Zhu L, Plow EF, Qin J. 2021. Initiation of focal adhesion assembly by talin and kindlin: A dynamic view. *Protein Sci* **30**:531-542. doi: 10.1002/pro.4014.

Figure 1

Live imaging shows Cas clusters mark sites of future vinculin clusters

(**A**) *Cas* wildtype and *Cas*^{mSc} genomic organization and *Cas*^{mSc} mRNA structure. (**B**) Representative immunoblot showing the pY410Cas, total Cas and vinculin (VCL) in control (Ctrl) and Cas^{mSc} MCF10A cells. (**C**) Cas^{mSc} co-localization with YFP-VCL. Cas^{mSc} MCF10A cells expressing YFP-VCL plated on COLI-treated glass-bottom dish for 30 min and visualized by TIRF microscopy. (**D-E**) Cas^{mSc} clusters form before vinculin clusters. TIRF microscopy of Cas^{mSc} YFP-VCL cells. Upper panels: individual time frames from (**D**) spreading or (**E**) migrating cells. Arrowheads indicate a Cas^{mSc} cluster (magenta) that is later joined by YFP-VCL (green). Lower panels: kymographs. (**F**) Pipeline for tracking ROIs. Upper panels: Raw images, false-colored Cas^{mSc} magenta and YFP-VCL green, from TIRF microscopy of spreading Cas^{mSc} YFP-VCL cells. Lower panels: masks showing tracked ROIs, color coded by time of onset. (**G**). Median $\Delta t_{1/2}$ (VCL-Cas) of multiple ROIs from n=19 spreading cells. Error bars show mean (43.8 s) and SEM (3 s). (**H**) Median $\Delta t_{1/2}$ (VCL-Cas) of multiple ROIs from n=13 spreading cells. Error bars show mean (68.5 s) and SEM (7 s).

Figure 1

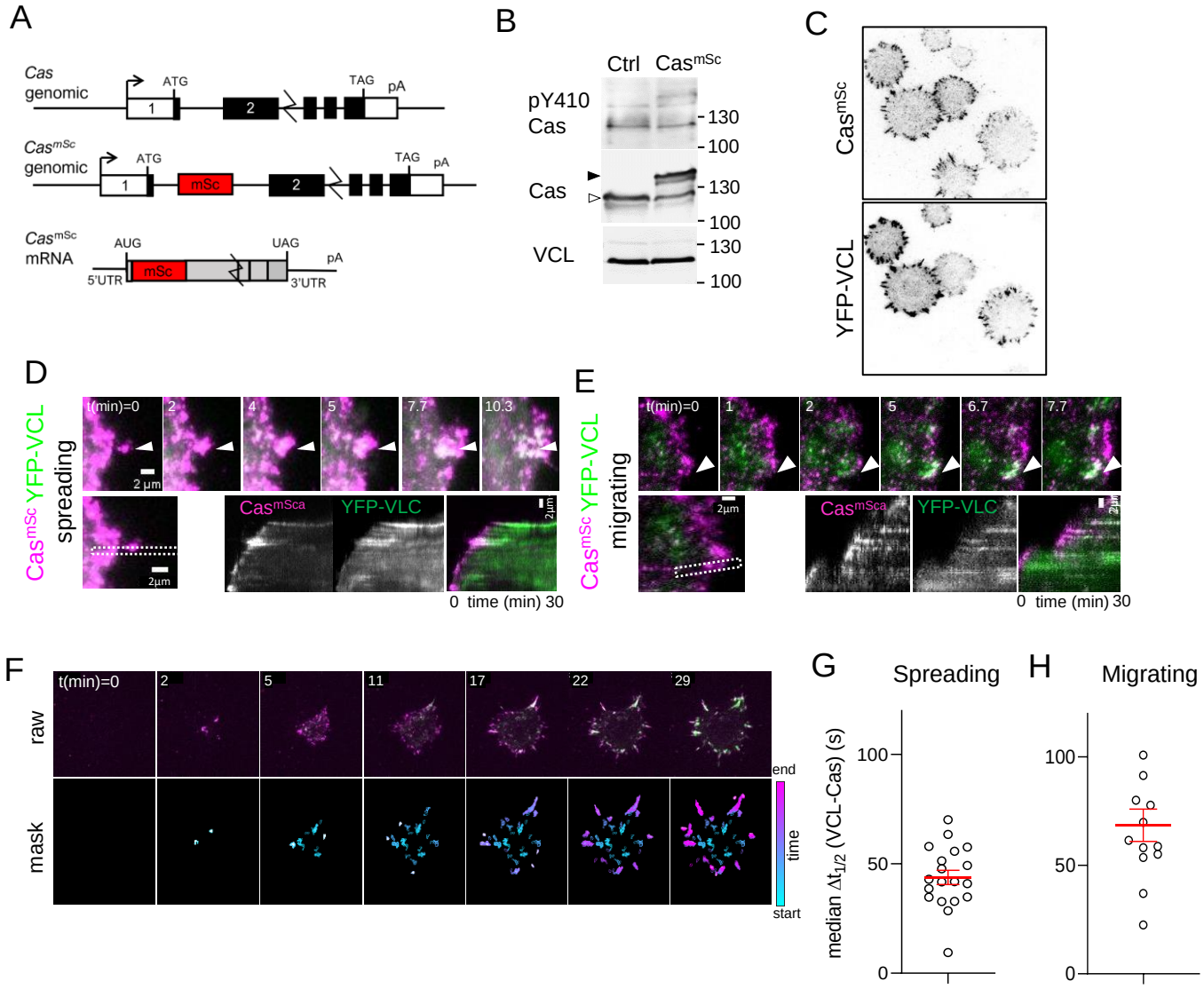
A
Cas genomic
ATG
TAG
pA
1
2
Cas^mSc genomic
mSc
Cas^mSc mRNA
AUG
UAG
5'UTR
3'UTR
B
Ctrl
Cas^mSc
pY410 Cas
Cas
VCL
130
100
C
Cas^mSc
YFP-VCL
D
Cas^mSc YFP-VCL
spreading
t(min)=0
2
4
5
7.7
10.3
2 µm
Cas^mSca
YFP-VLC
0 time (min) 30
E
migrating
1
6.7
F
raw
mask
11
17
22
29
end
time
start
G
Spreading
H
Migrating
median Δt1/2 (VCL-Cas) (s)
100
50
0

Figure 1 – figure supplement 1

Vector design and validation of Cas^{mSc} tagging

(**A**) Overview of the modified pORANGE-based system for tagging endogenous *Cas* at the N-terminal end by inserting an artificial exon. T, target sequence; PAM, protospacer adjacent motif; SA, splice acceptor; SD, splice donor, SpCas9, *Streptococcus pyrogenes* Cas9. (**B**) Primer positions and PCR products amplified from *Cas*^{WT} and *Cas*^{mSc} genomic DNA. (**C**) Sanger sequencing of *Cas*^{WT} (amplified with primers a+b) and 5' and 3' junctions of *Cas*^{mSc} (amplified with a+d and c+b respectively) genomic DNA. Note poor sequencing and inserted base indicative of imprecise insertion. (**D**) Primer positions and PCR products amplified from *Cas*^{WT} and *Cas*^{mSc} cDNA. (**E**) Sanger sequencing of RT-PCR amplified products from exon-exon junctions of *Cas*^{WT} (primers a+b) and *Cas*^{mSc} (primers a+d and c+b respectively) cDNA. Note in-frame *mSc* sequence between *Cas* codons 4 and 5.

Figure 1 – figure supplement 1

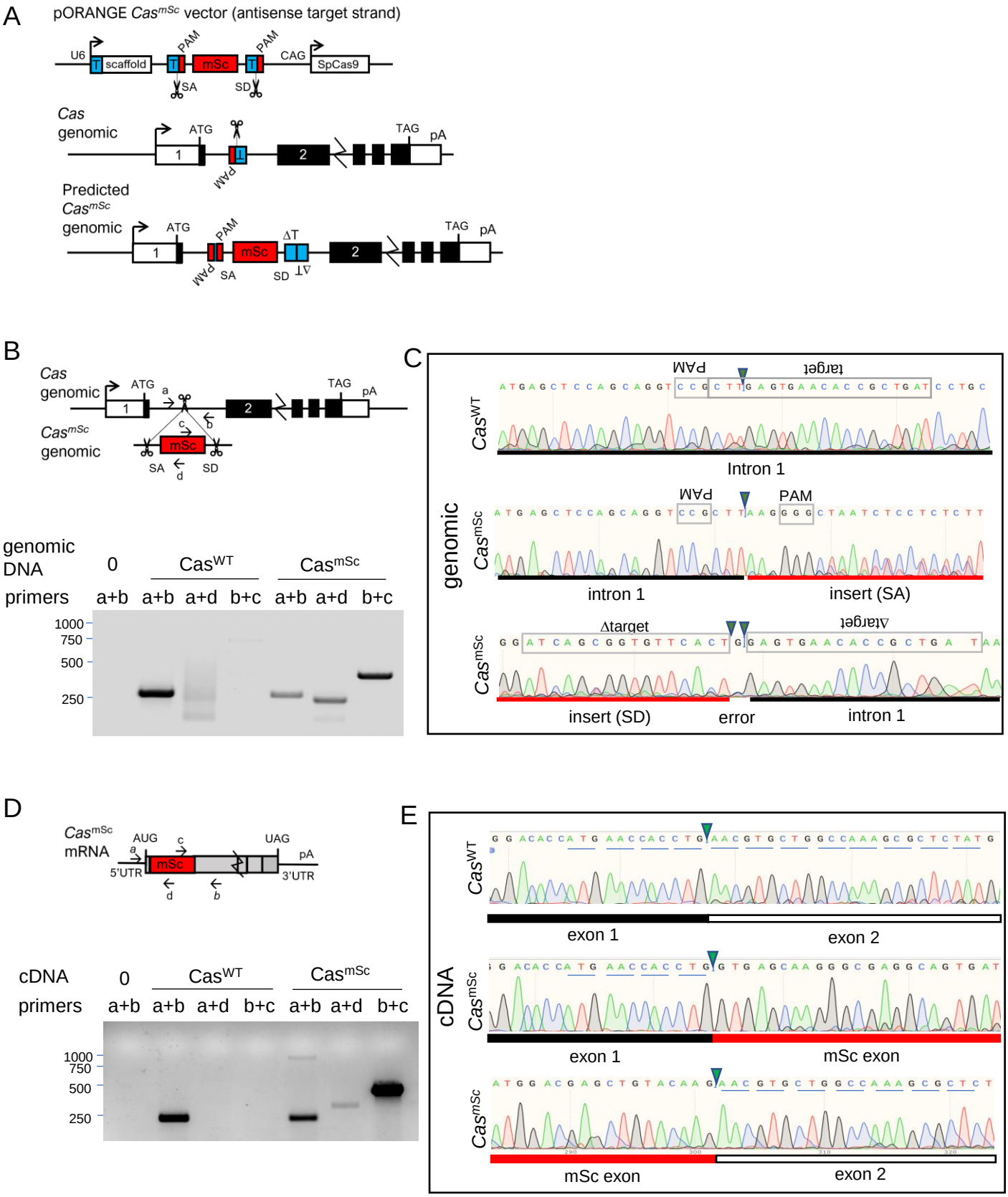

Figure 1 – figure supplement 2

Time interval between Cas and vinculin cluster assembly

(**A**) Normalized intensity profiles of multiple YFP-VCL and Cas^{mSc} ROIs tracked over 30 min of spreading in a single cell. Frame interval 20s. Each line tracks mean intensity of an ROI ≥20 pixels (0.5 μm^2) in area. (**B**) Paired intensity profiles for YFP-VCL and Cas^{mSc} in a single tracked ROI. $\Delta t_{1/2}$ was calculated by subtracting $t_{1/2}$ of normalized intensity for YFP-VCL from Cas^{mSc} of the same ROI. (**C**) $\Delta t_{1/2}$ (VCL-Cas) for 73 ROIs in a single spreading Cas^{mSc} YFP-VCL MCF10A cell. Error bars indicate median (58.1 s) and 95% confidence interval (19.7-96.9 s). (**D**) $\Delta t_{1/2}$ (VCL-Cas) for 90 ROIs in a single migrating Cas^{mSc} YFP-VCL MCF10A cell. Error bars indicate median (54.8 s) and 95% confidence interval (23-105 s). (**E**) $\Delta t_{1/2}$ (VCL-Cas) for 37 ROIs in a single spreading Cas^{mSc} YFP-VCL HeLa cell. Error bars indicate median (66.2 s) and 95% confidence interval (21-114 s). (**F**) Median $\Delta t_{1/2}$ (VCL-Cas) for n=4 spreading Cas^{mSc} YFP-VCL HeLa cells. Error bars indicate mean (44.1 s) and SEM (9 s).

Figure 1 – figure supplement 2

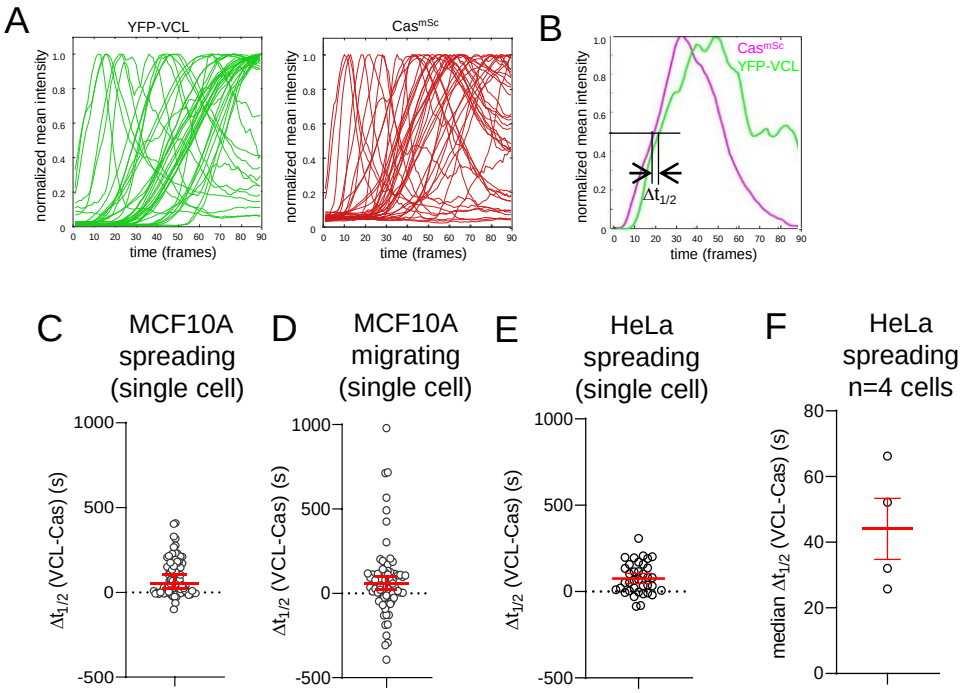

Figure 2

Cas clusters precede vinculin clusters independent of ECM

(**A**) Integrin specificity of different ECM. Representative images and mean spread areas of Cas^{mSc} MCF10A cells plated for 30 min on fibronectin- or COLI-coated surface and stained with phalloidin. Cas^{mSc} MCF10A cells were treated with blocking antibodies α5β1 (P8D4) and α2β1 (P1E6) during spreading on fibronectin- or collagen-coated glass for 30 min. Cells were then fixed and stained with phalloidin to visualize F-actin. (**B**) Staining for active-β1 using conformation-specific antibodies 9EG7. Ventral section. Mean β1 cluster area and intensity were calculated from 5-6 cells containing >50 clusters of ≥20 pixels area. (**C**) Median $\Delta t_{1/2}$ (VCL-Cas) n=7-13 spreading Cas^{mSc} YFP-VCL MCF10A cells on fibronectin or collagen. Error bars indicate mean and SEM. ns, nonsignificant by Mann-Whitney test.

Figure 2

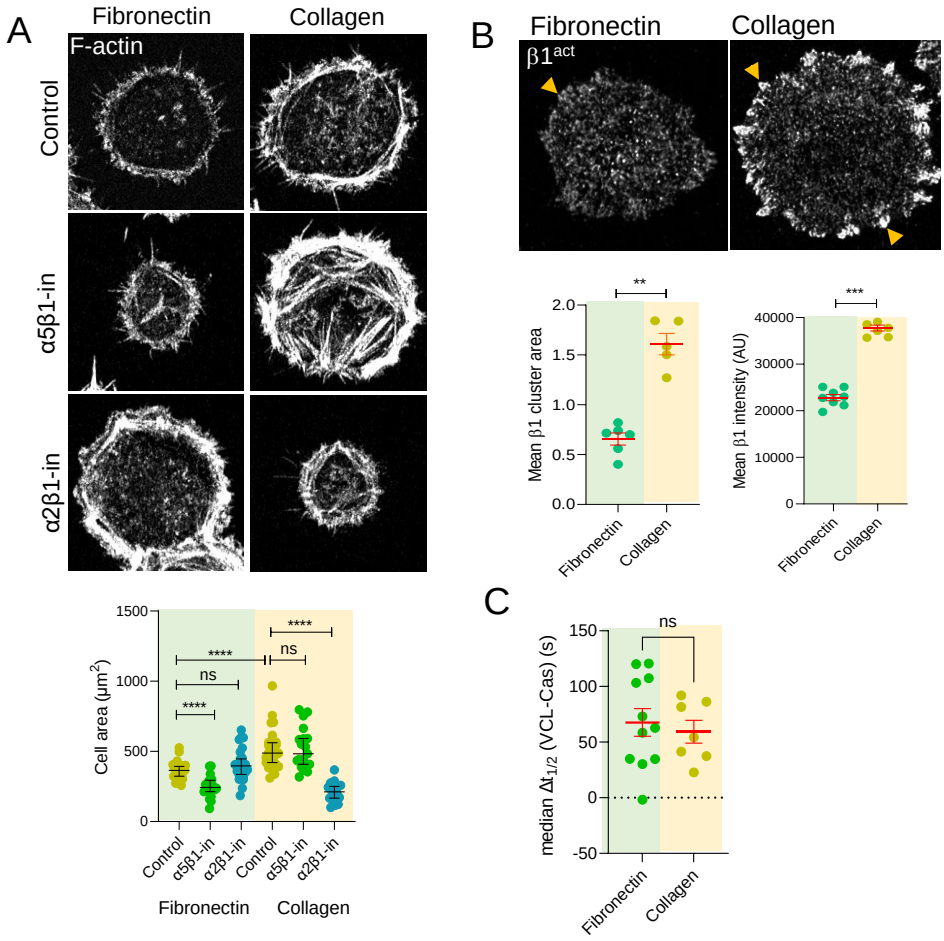
A
Fibronectin
Collagen
F-actin
Control
α5β1-in
α2β1-in
B
Fibronectin
Collagen
β1act
Mean β1 cluster area
Mean β1 intensity (AU)
Fibronectin
Collagen
C
Cell area (μm2)
Control
α5β1-in
α2β1-in
Control
α5β1-in
α2β1-in
Fibronectin
Collagen
median Δt1/2 (VCL-Cas) (s)
ns
Fibronectin
Collagen

Figure 3

Live imaging shows Cas clusters mark sites of future integrin clusters

(**A**) Cas^{mSc} clusters form before β1Ecto-pH clusters. TIRF microscopy of spreading Cas^{mSc} β1Ecto-pH MCF10A cells. Upper panels: individual time frames. Arrowheads indicate a Cas^{mSc} cluster (magenta) that is later joined by β1Ecto-pH (green). Lower panels: kymographs. (**B**) Median $\Delta t_{1/2}$ (β1-Cas) of multiple ROIs from 12 spreading Cas^{mSc} β1Ecto-pH MCF10A cells. Error bars show mean (67.33 s) and SEM (9.4 s). (**C**) *ITGB1* wildtype and *ITGB1*^{GFP} genomic organization and *ITGB1*^{GFP} mRNA structure. (**D**) Immunoblot showing expression of $ITGB1^{GFP}$ protein in Cas^{mSc} $ITGB1^{GFP}$ HeLa cells. (**E**) Cas^{mSc} clusters form before $ITGB1^{GFP}$ clusters. TIRF microscopy of Cas^{mSc} $ITGB1^{GFP}$ HeLa cells. Upper panels: individual time frames. Arrowheads indicate a Cas^{mSc} cluster (magenta) that is later joined by $ITGB1^{GFP}$ (green). Lower panels: kymographs. (**F**). Median $\Delta t_{1/2}$ (ITGB1-Cas) of multiple ROIs from 11 spreading Cas^{mSc} $ITGB1^{GFP}$ HeLa cells. Error bars show mean (62.9 s) and SEM (7.2 s).

Figure 3

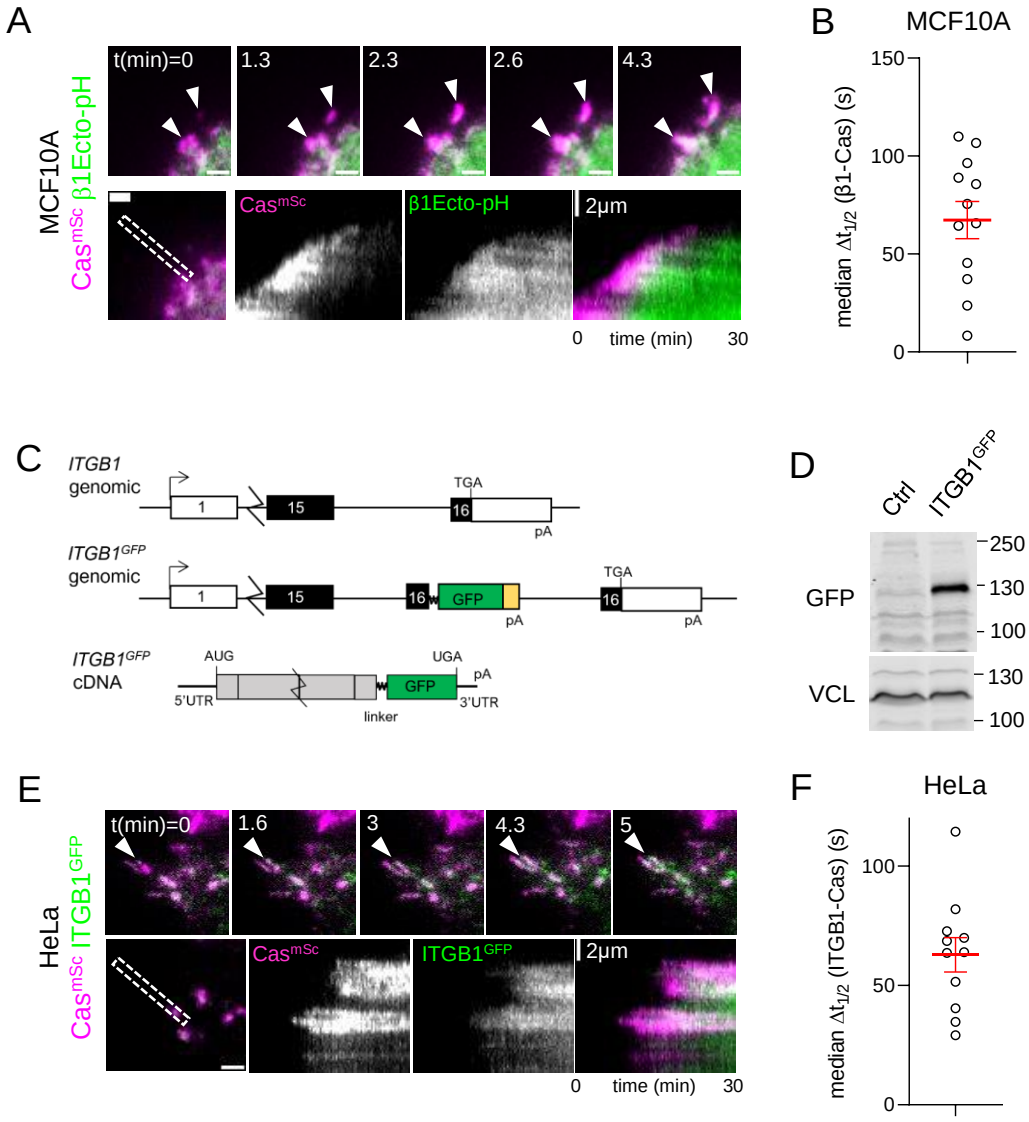
A
MCF10A
Cas^mSc β1Ecto-pH
t(min)=0
1.3
2.3
2.6
4.3
Cas^mSc
β1Ecto-pH
2µm
0
time (min)
30
B
MCF10A
median Δt1/2 (β1-Cas) (s)
150
100
50
0
C
ITGB1 genomic
1
15
16
TGA
pA
ITGB1^GFP genomic
GFP
ITGB1^GFP cDNA
AUG
UGA
5'UTR
linker
3'UTR
D
Ctrl
ITGB1^GFP
GFP
VCL
250
130
100
E
HeLa
Cas^mSc ITGB1^GFP
t(min)=0
1.6
3
4.3
5
Cas^mSc
ITGB1^GFP
2µm
0
time (min)
30
F
HeLa
median Δt1/2 (ITGB1-Cas) (s)
100
50
0

Figure 3 – figure supplement 1

Vector design and validation of ITGB1^{GFP} tagging

(**A**) Overview of the modified pORANGE-based system for tagging endogenous *ITGB1* at the C-terminal end by inserting an artificial exon and 3' end signal. T, target sequence; PAM, protospacer adjacent motif; SA, splice acceptor; SD, splice donor, SpCas9, *Streptococcus pyrogenes* Cas9; pA, SV40 3' end and poly A signal sequence. (**B**) Primer positions and PCR products amplified from *ITGB1^{WT}* and *ITGB1^{GFP}* genomic DNA. (**C**) Sanger sequencing of *ITGB1^{WT}* (amplified with primers a+b) and 5' and 3' junctions of *ITGB1^{GFP}* (amplified with a+d and c+b respectively) genomic DNA. Note poor sequencing and deletion indicative of imprecise insertion. (**D**) Primer positions and PCR products amplified from *ITGB1^{WT}* and *ITGB1^{GFP}* cDNA. (**E**) Sanger sequencing of RT-PCR amplified product from exon-exon junction of *ITGB1^{GFP}* (primers a'+b') cDNA. Note in-frame *ITGB1* sequence between exon 15 and the introduced exon 16-GFP fusion.

Figure 3 – figure supplement 1

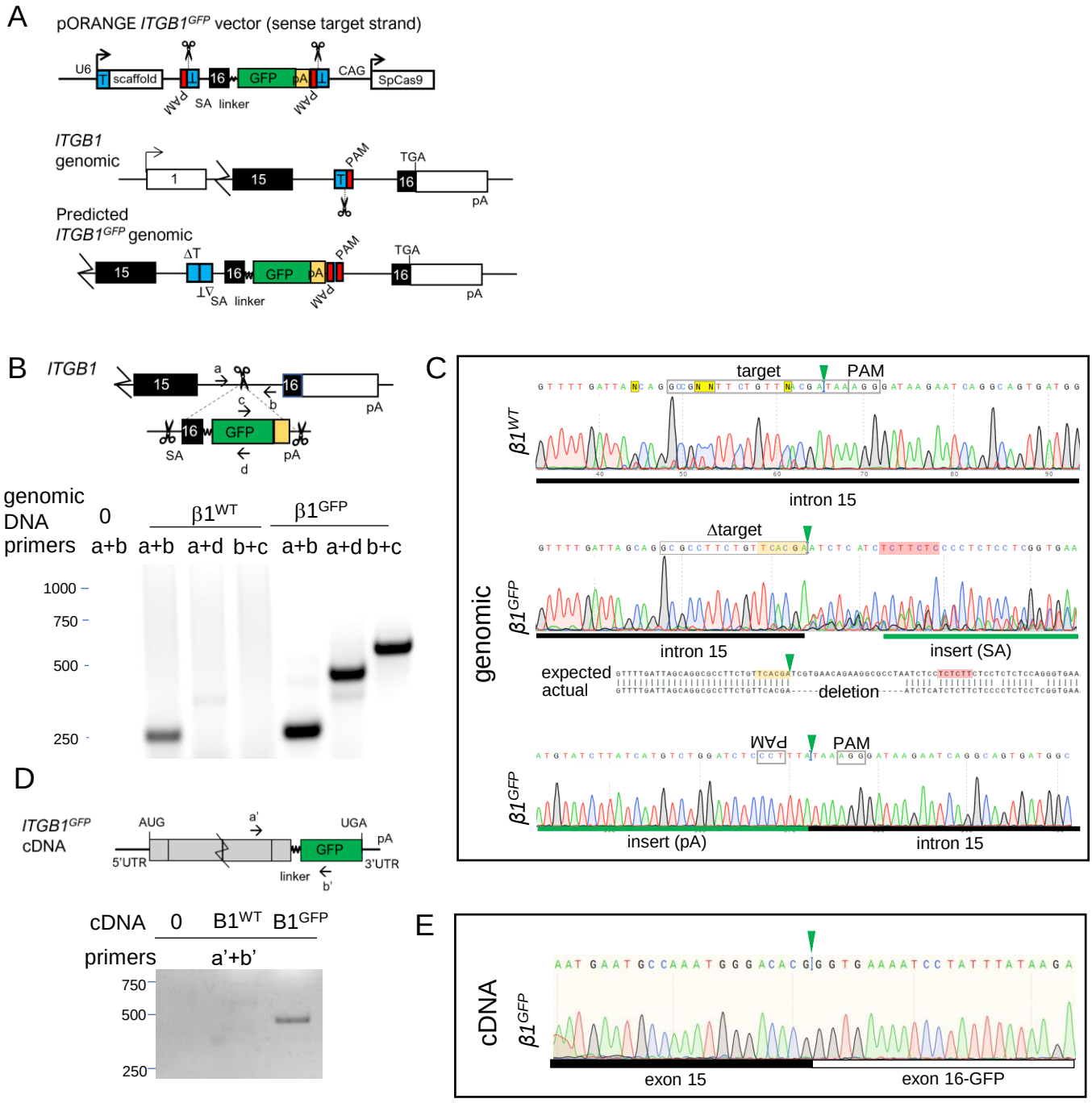

Figure 4

Initial Cas clusters contain Crk

(**A**) *Crk* wildtype and *Crk*^{mGL} genomic organization and *Crk*^{mGL} mRNA structure. (**B**) Immunoblot showing expression of Crk^{mGL} protein in Crk^{mGL} HeLa cells. (**C**) Crk^{mGL} clusters form shortly after Cas^{mSc} clusters. TIRF microscopy of Cas^{mSc} Crk^{mGL} HeLa cells. Upper panels: individual time frames. Arrowheads indicate a Cas^{mSc} cluster (magenta) that is rapidly joined by Crk^{mGL} (green). Lower panels: kymographs. (**D**) Median $\Delta t_{1/2}$ (Crk-Cas) of multiple ROIs from eight spreading Cas^{mSc} Crk^{mGL} HeLa cells. Error bars show mean (5 s) and SEM (3.9 s). (**E**) Median $\Delta t_{1/2}$ (Crk-Cas) of multiple ROIs from 4-6 spreading Cas^{mSc} Crk^{mGL} HeLa control and eCF506-treated cells. Error bars show mean and SEM. *, $P<0.05$ by Mann Whitney U test.

Figure 4

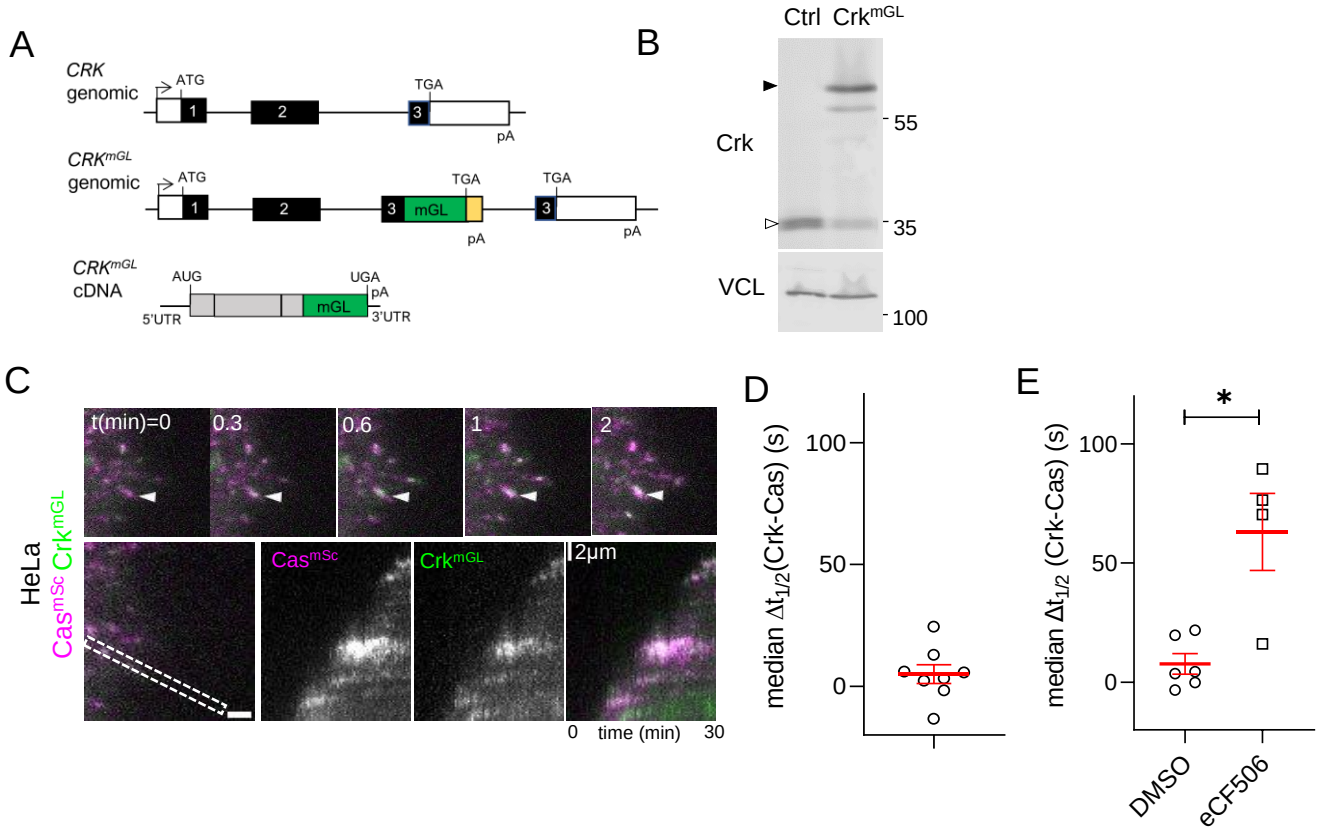
A
CRK genomic
ATG
TGA
1
2
3
pA
CRKmGL genomic
ATG
TGA
TGA
1
2
3
mGL
3
pA
pA
CRKmGL cDNA
AUG
UGA
pA
mGL
5'UTR
3'UTR
B
Ctrl
CrkmGL
Crk
55
35
VCL
100
C
t(min)=0
0.3
0.6
1
2
HeLa
CasmSc CrkmGL
CasmSc
CrkmGL
2µm
0
time (min)
30
D
median Δt1/2(Crk-Cas) (s)
100
50
0
E
*
median Δt1/2 (Crk-Cas) (s)
100
50
0
DMSO
eCF506

Figure 4 – figure supplement 1

Vector design and validation of Crk^{mGL} tagging

(**A**) Overview of the modified pORANGE-based system for tagging endogenous *Crk* at the C-terminal end by inserting an artificial exon and 3' end signal. T, target sequence; PAM, protospacer adjacent motif; SA, splice acceptor; SD, splice donor, SpCas9, *Streptococcus pyrogenes* Cas9; pA, SV40 3' end and poly A signal sequence. (**B**) Primer positions and PCR products amplified from *Crk^{WT}* and *Crk^{mGL}* genomic DNA. (**C**) Sanger sequencing of *Crk^{WT}* (amplified with primers a+b) and 5' and 3' junctions of *Crk^{mGL}* (amplified with a+d and c+b respectively) genomic DNA. Note poor sequencing and deletion indicative of imprecise insertion. (**D**) Primer positions and PCR products amplified from *Crk^{WT}* and *Crk^{mGL}* cDNA. (**E**) Sanger sequencing of RT-PCR amplified product from exon-exon junction of *Crk^{mGL}* (primers a'+b') cDNA. Note in-frame *Crk* sequence between exon 2 and the introduced exon 3-mGL fusion.

Figure 4 – figure supplement 1

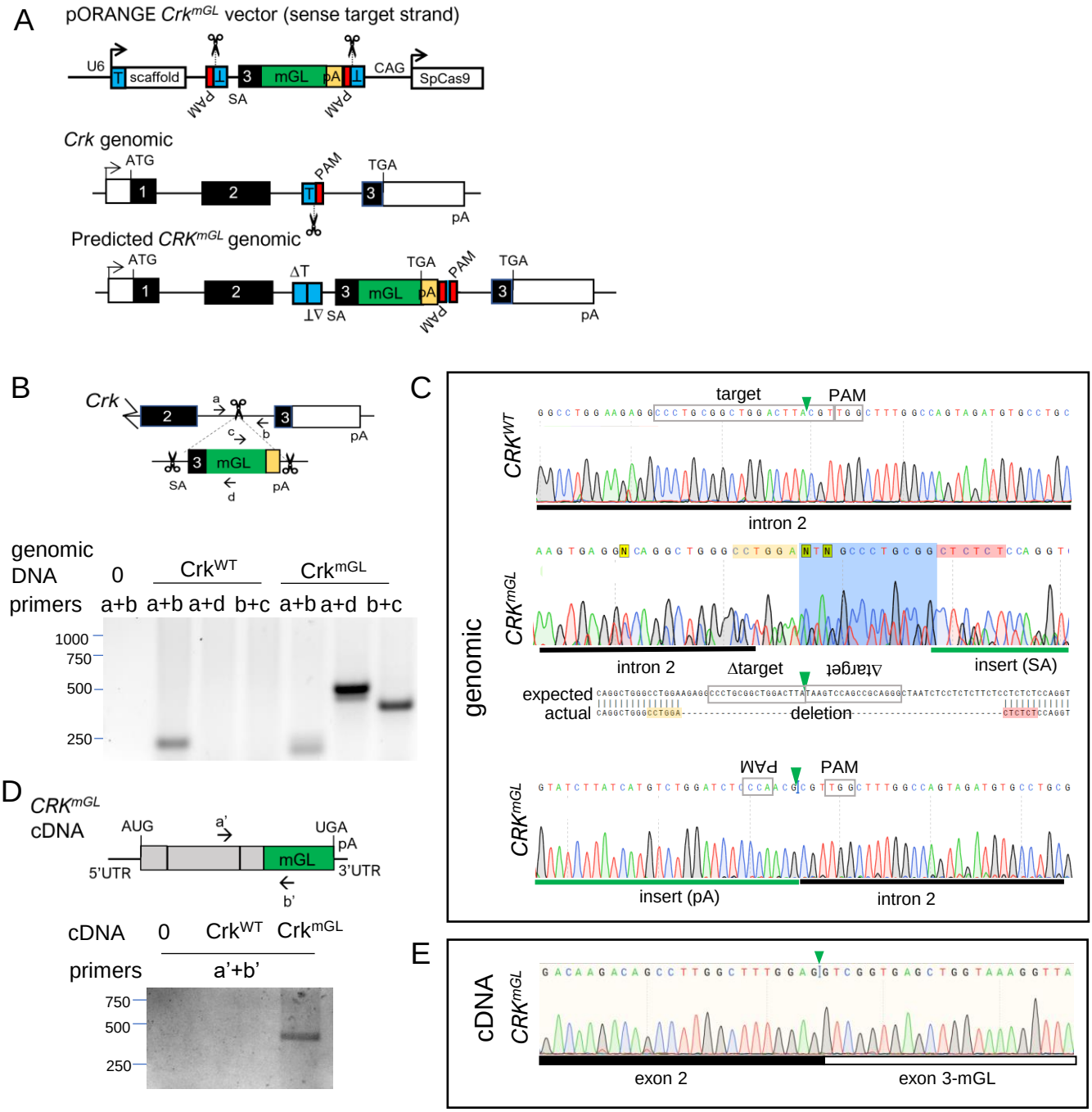

Figure 5

Spatial distribution of integrin adhesion proteins in Cas clusters

(**A**) Representative image used for measuring spatial distribution of proteins and phosphoproteins across developing focal adhesions. Cas^{mSc} YFP-VCL MCF10A cells were fixed and imaged by TIRF after 30 min spreading. Inset shows 4 x 0.8 μm region, starting from cell edge to towards cell center, used to graph mean intensity against distance. (**B**) Mean intensity against distance plot for Cas^{mSc} and YFP-VCL across ≥20 regions from several cells. Error bars indicate mean and SEM. (**C**) Heat map of normalized mean immunofluorescence intensity against distance for various antigens in Cas^{mSc} MCF10A stained with indicated antibodies. (**D**) Model showing inferred progression from initial nascent adhesions or focal complexes containing high levels of pY410Cas, inactive integrin and pY861FAK, progressing to become focal adhesions containing low levels of Cas and high levels of active integrin, vinculin, pY397FAK, F-actin, talin, paxillin and kindlin.

Figure 5

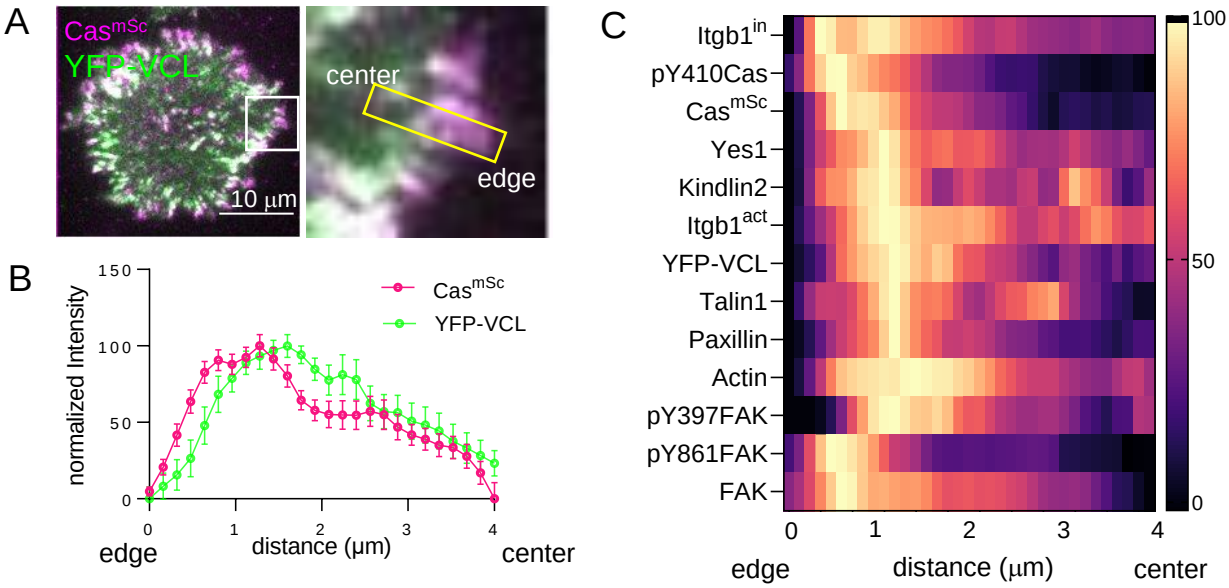
A
Cas^mSc
YFP-VCL
10 µm
center
edge
B
normalized Intensity
150
100
50
0
Cas^mSc
YFP-VCL
0
1
2
3
4
edge
distance (µm)
center
C
Itgb1^in
pY410Cas
Cas^mSc
Yes1
Kindlin2
Itgb1^act
YFP-VCL
Talin1
Paxillin
Actin
pY397FAK
pY861FAK
FAK
100
50
0
0
1
2
3
4
edge
distance (µm)
center

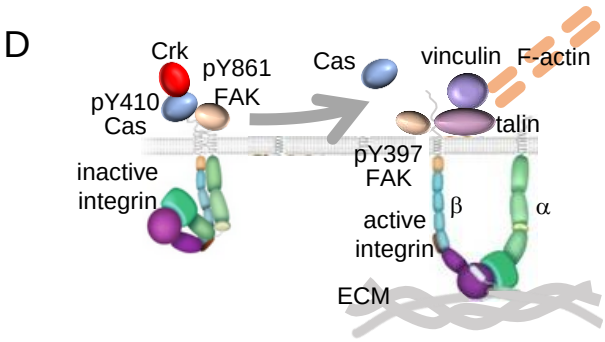
D
Crk
pY861
FAK
pY410
Cas
Cas
vinculin
F-actin
talin
pY397
FAK
inactive
integrin
active
integrin
β
α
ECM

Figure 5 – figure supplement 1

Representative images showing spatial distribution of adhesion proteins in Cas clusters

(A) Cas^{mSc} MCF10A cell stained for pY410Cas, inactive integrin β1, and F-actin. (B) Cas^{mSc} YFP-VCL MCF10A cell stained for pY410Cas and active integrin β1.

Figure 5 – figure supplement 1

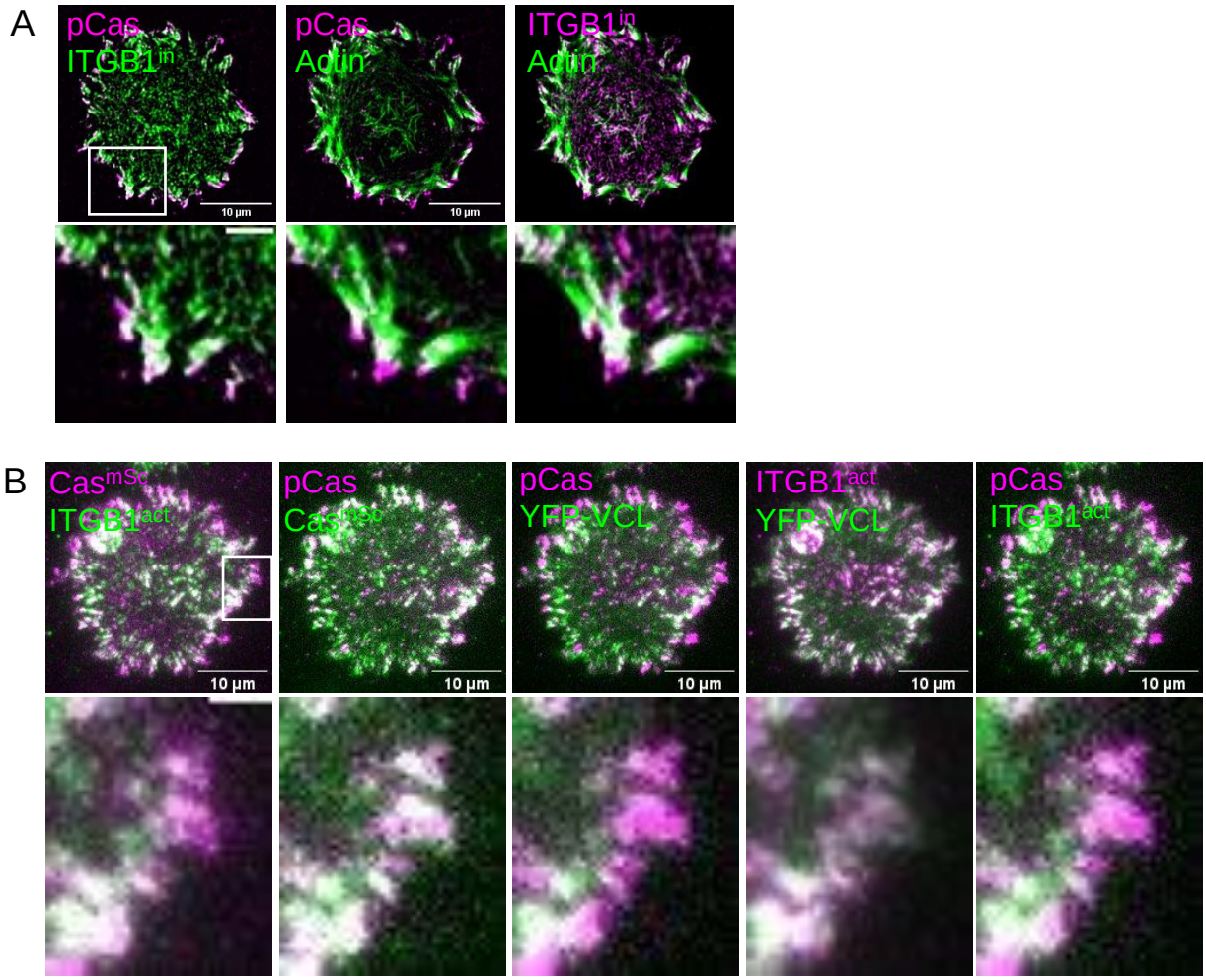

Figure 5 – figure supplement 2

Phosphorylated Cas is enriched in the adhesome

(A-B) Representative results from two independent experiments. Western blots of total (T), supernatant (S), and adhesome (A) fractions from cells plated on different ECM for 60 min were probed with the indicated antibodies. PDL, poly-D-lysine; COLI, collagen-I. (**C**) Quantification of multiple independent experiments. Proportion adhesome was calculated from A/(S+A). Error bars indicate mean and SD.

Figure 5 – figure supplement 2

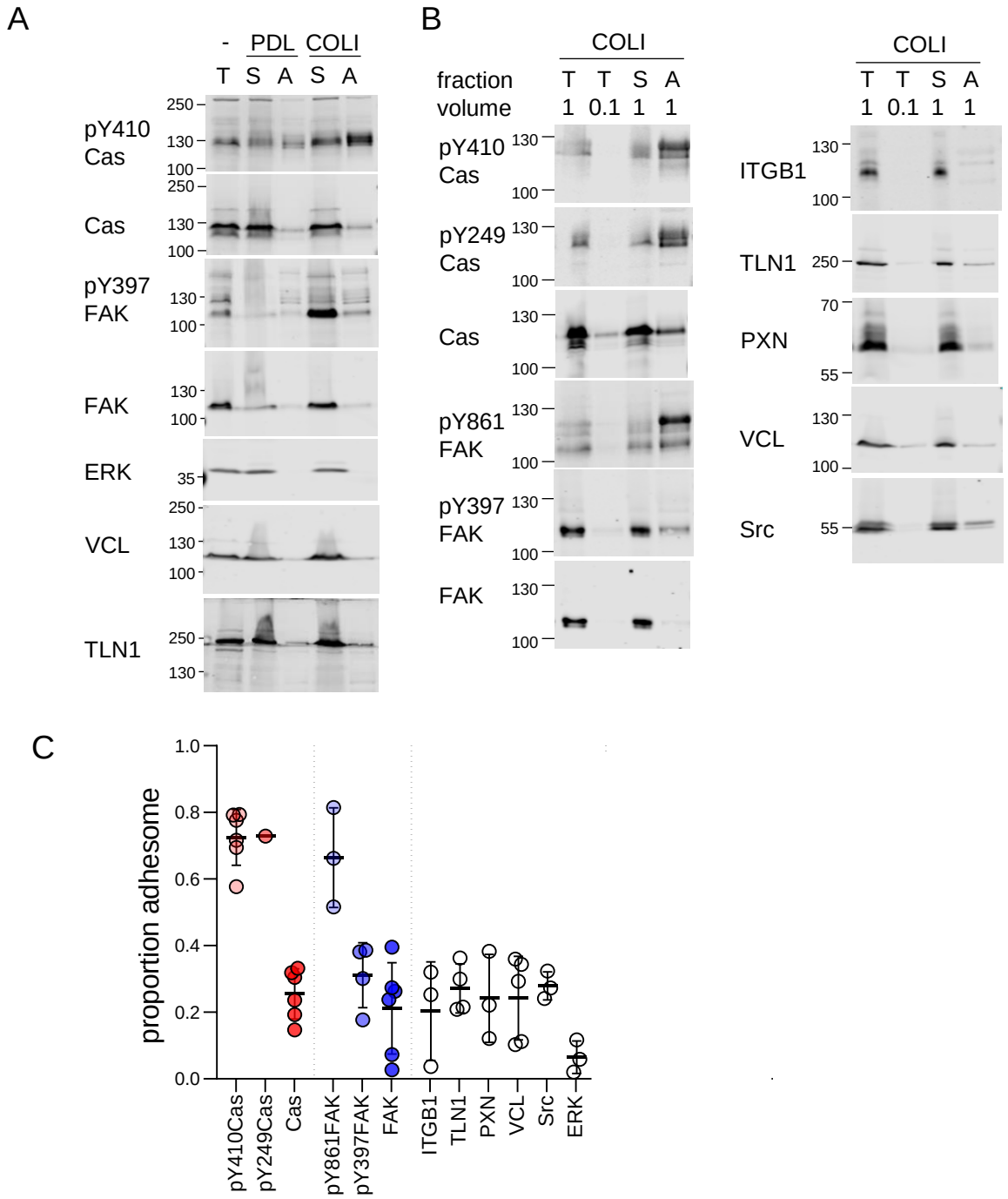

Figure 6

Cas regulates vinculin recruitment and focal adhesion assembly

(**A**) Representative images (ventral section) of Cas^{mSc} YFP-VCL MCF10A cells treated with control, Cas or vinculin siRNA and fixed after 30 min of spreading. (**B**) Quantification of mean cell area and the number, mean Cas intensity, and mean vinculin intensity of individual Cas and/or vinculin clusters. Error bars show mean and SEM for n=10-50 cells from three biological repeats. ns, non-significant; *, P<0.05; **, P<0.01; ***, P<0.001; ****, P<0.0001 by Kruskal-Wallis followed by Dunn's multiple comparison test. (**C**) Representative images of MCF10A expressing YFP-VCL cells treated with control or Cas siRNA and fixed after spreading in the absence or presence of Mn^{2+} for 30 min. Graphs show the mean cell spread area and mean intensity of YFP-VCL clusters. Error bars show mean and SEM for n=6-20 cells from two biological repeats. P values from pairwise Mann Whitney U tests, comparing each test condition to the control shown.

Figure 6

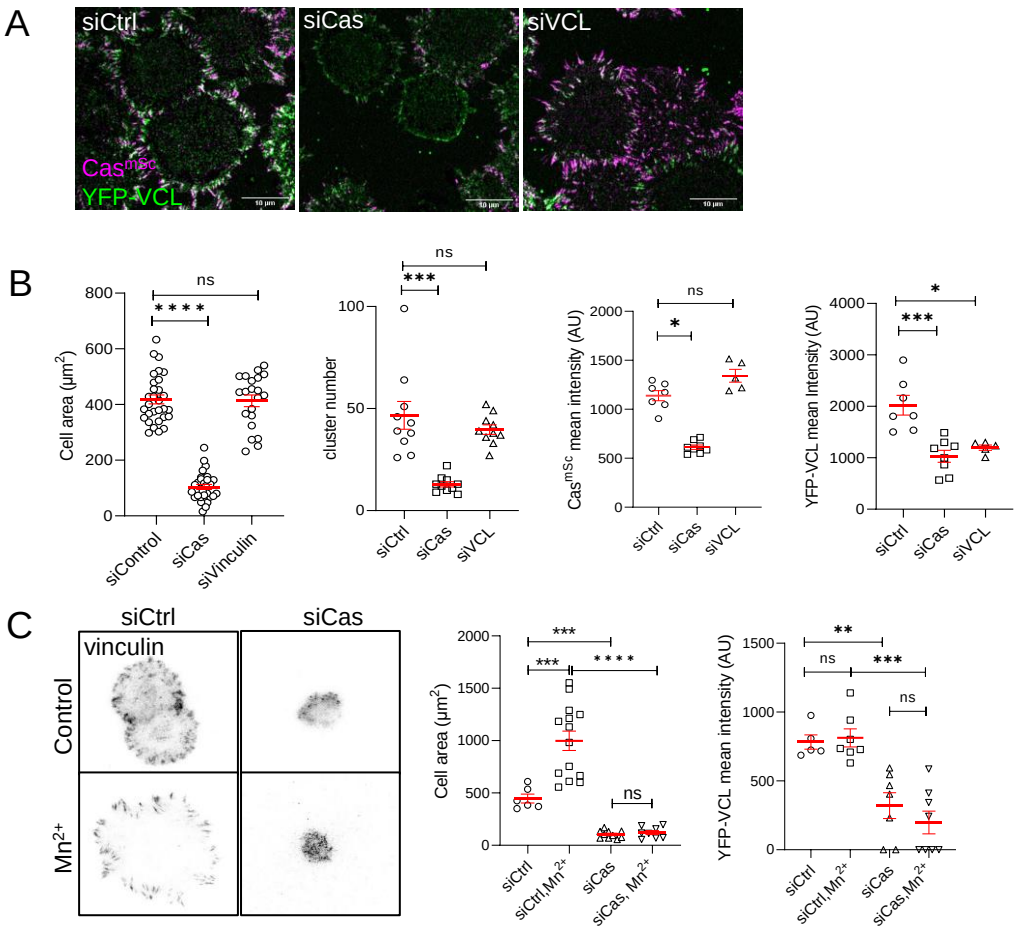
A
siCtrl
siCas
siVCL
Cas^mSc
YFP-VCL
B
Cell area (µm²)
cluster number
Cas^mSc mean intensity (AU)
YFP-VCL mean Intensity (AU)
siControl
siCas
siVinculin
siCtrl
siVCL
ns
C
siCtrl
siCas
vinculin
Control
Mn²⁺
Cell area (µm²)
YFP-VCL mean intensity (AU)
siCtrl,Mn²⁺
siCas, Mn²⁺

Figure 6 – figure supplement 1

Cas depletion inhibits MCF10A cell migration

(**A**) Immunoblot of cell lysates, (**B**) wind-rose plots depicting total path traveled (12 hrs), and (**C**) representative images (ventral section), of Cas^{mSc} YFP-VCL MCF10A cells treated with control or Cas siRNA. (**D**) Immunoblot of cell lysates harvested from Cas^{mSc} MCF10A cells treated with control or VCL siRNA.

Figure 6 – figure supplement 1

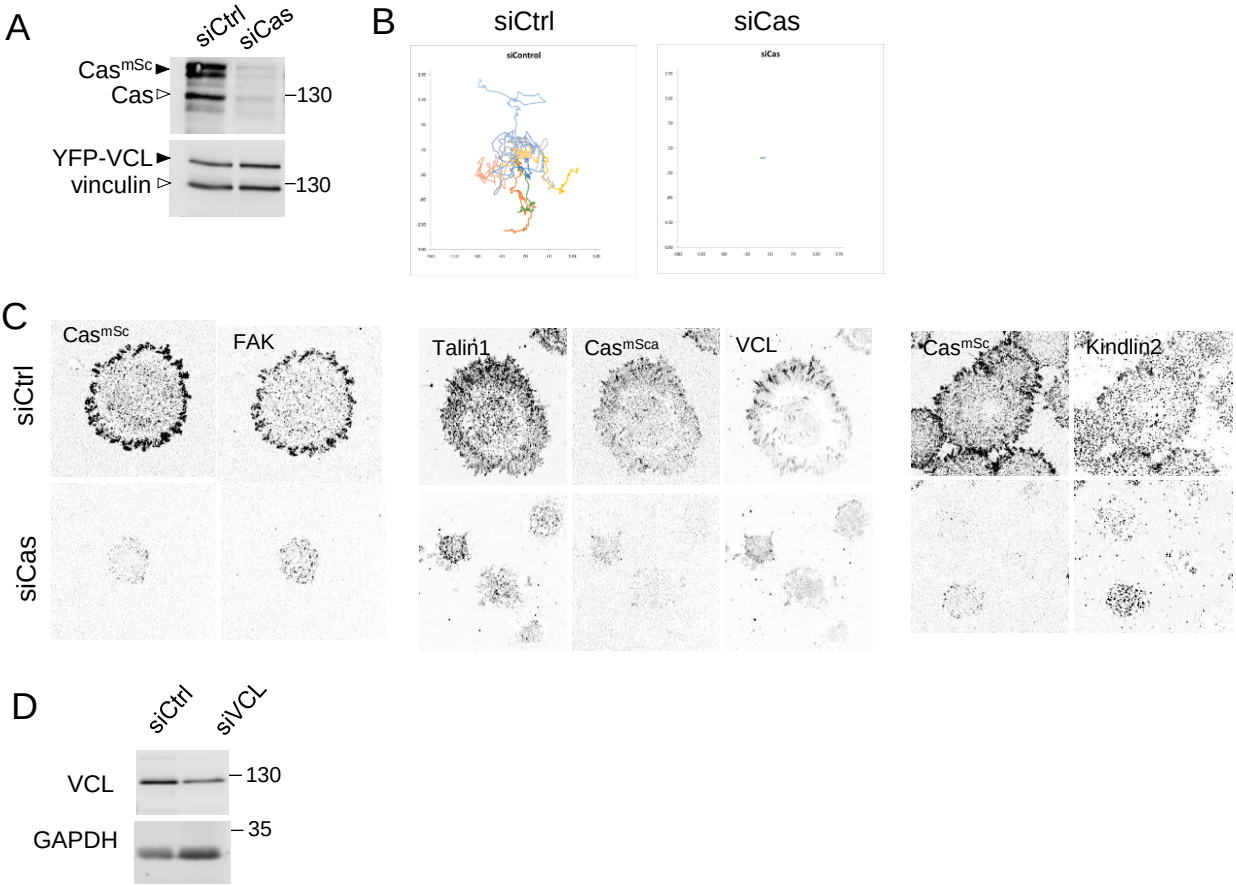

Figure 6 – figure supplement 2

Controls and additional data showing Cas regulates vinculin recruitment and focal adhesion assembly

(**A**) Representative endpoint dual-color time-lapse TIRF micrographs of spreading Cas^{mSc} YFP-VCL MCF10A cells treated with control, Cas or FAK siRNA; (**B**) Immunoblot showing FAK depletion. (**C**) Mean cell area, mean Cas^{mSc} and YFP-VCL intensity, and median $\Delta t_{1/2}$ (VCL-Cas) from 9-16 cells in three biological repeats. Error bars show mean and SEM. (**D**) Representative endpoint dual-color time-lapse TIRF micrographs of spreading Cas^{mSc} YFP-VCL MCF10A cells treated with control, talin1 or kindlin2 siRNA. (**E**) Immunoblot showing talin1 and kindlin2 depletion. (**F**) Mean cell area, mean Cas^{mSc} and YFP-VCL intensity, and median $\Delta t_{1/2}$ (VCL-Cas) from 5-12 cells in three biological repeats. ns, non-significant; *, P<0.05; **, P<0.01; ***, P<0.001; ****, P<0.0001 by Kruskal-Wallis followed by Dunn's multiple comparison test.

Figure 6 – figure supplement 2

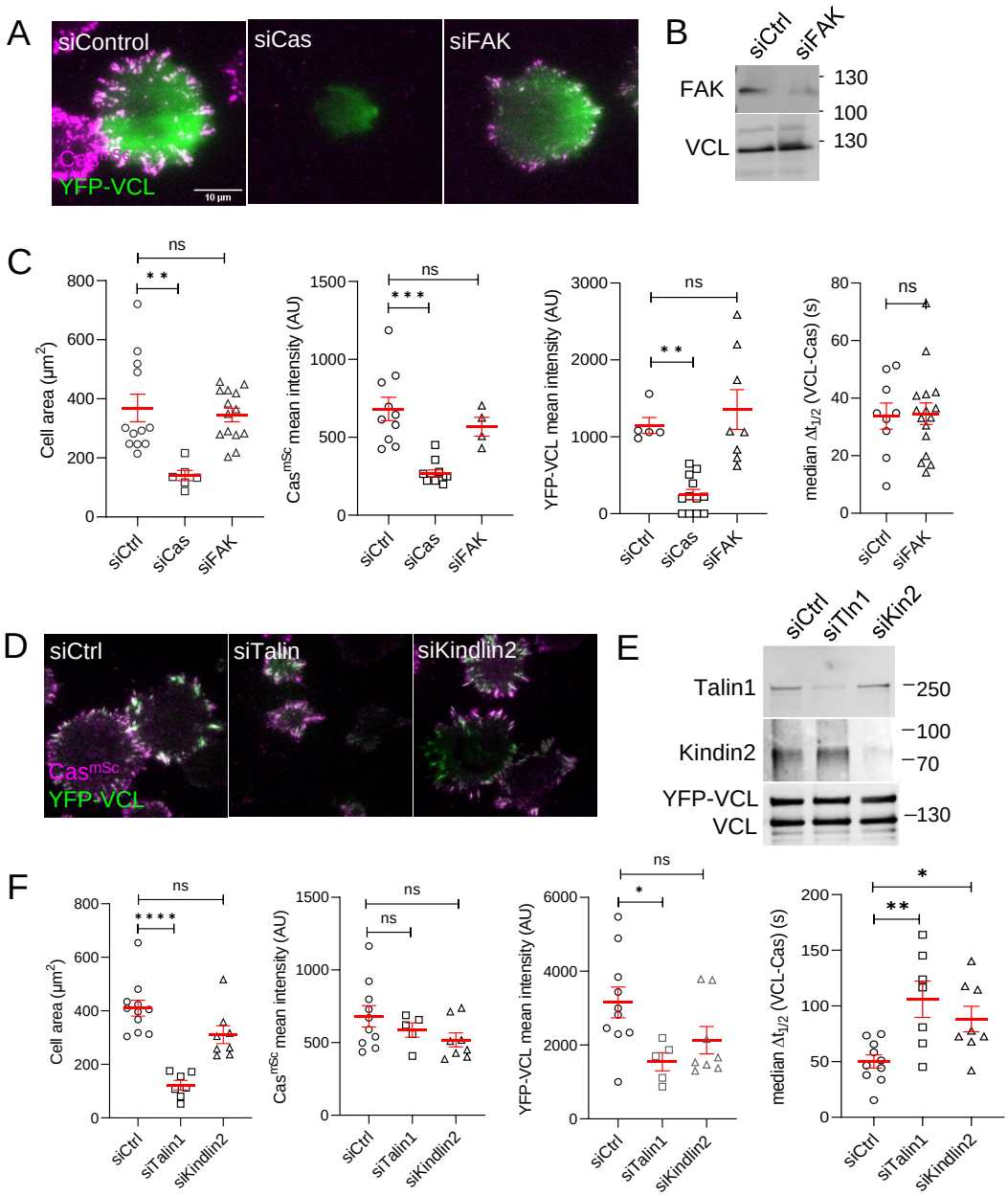

Figure 7

SFK-Cas-Crk-Rac1 signaling regulates adhesion assembly

(**A**) Median $\Delta t_{1/2}$ (VCL-Cas) from 7-11 time-lapse dual-color TIRF micrographs of spreading Cas^{mSc} YFP-VCL MCF10A cells treated with DMSO or SFK inhibitor eCF506 (left), or with control or Crk/CrkL siRNA (right). (**B**) Mean cluster intensity of the pY410Cas, Cas^{mSc} and YFP-VCL in Cas^{mSc} YFP-VCL MCF10A cells treated with control, Src, Fyn or Yes1 siRNA and fixed after 30 min of spreading. Error bars show mean and SEM from n=7-10 cells from three biological repeats. (**C**) Representative endpoint dual-color time-lapse TIRF micrographs (left) and quantification (right) of spreading Cas^{mSc} YFP-VCL MCF10A cells treated with DMSO or Rac1 inhibitor EHT1864. Error bars show mean and SEM of 6-12 cells in 3 biological repeats. (**D-E**) Representative FRET ratio images (left) and quantification (right) of Rac1-2G biosensor MCF10A cells treated with (**D**) control or Cas, or (**E**) control or Yes1 siRNA and fixed after 30 min of spreading. Error bars show mean and SEM from >30 cells from 3 biological replicates. All P values by Mann Whitney U tests.

Figure 7

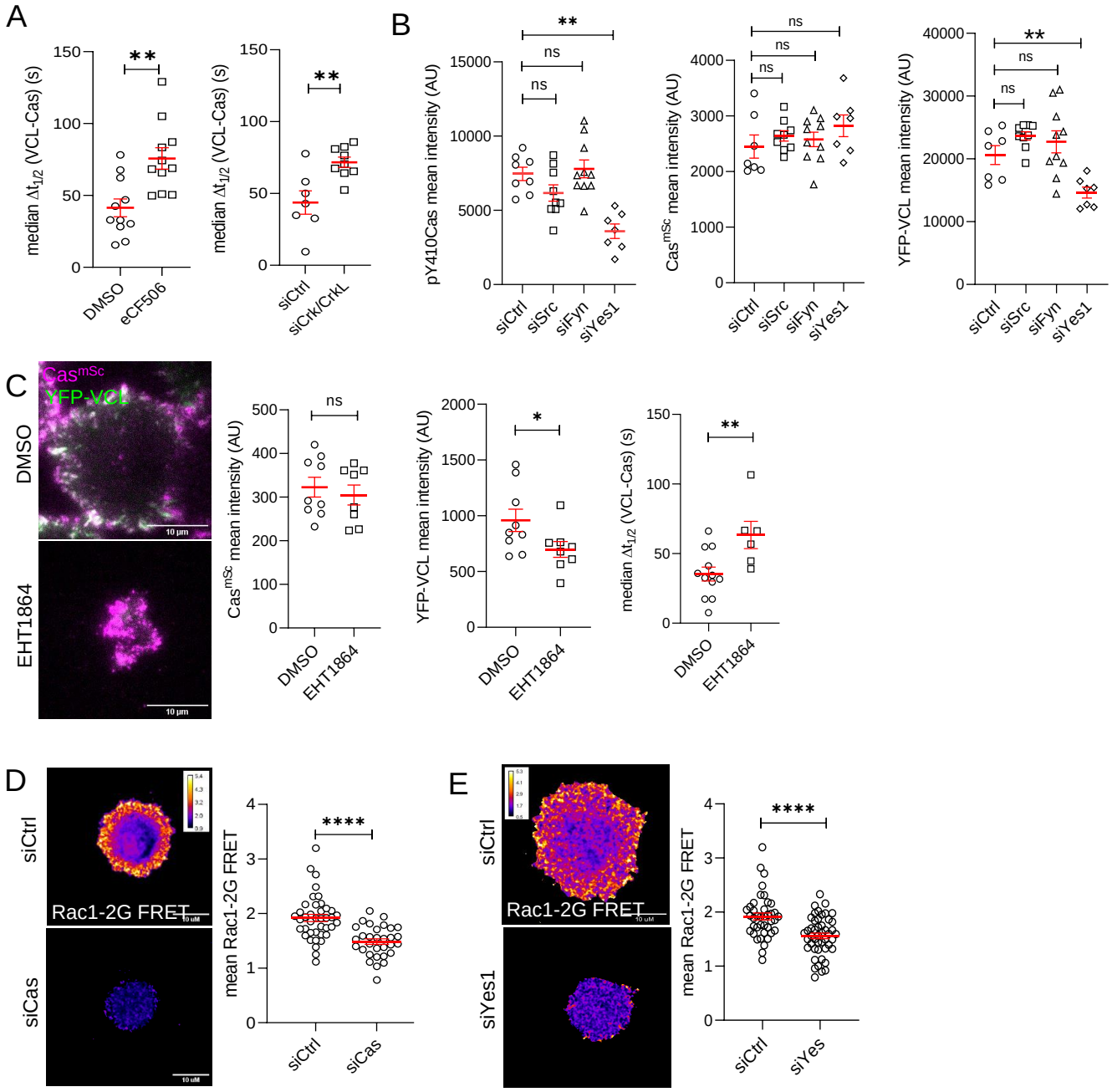
A
median Δt1/2 (VCL-Cas) (s)
DMSO
eCF506
siCtrl
siCrk/CrkL
B
pY410Cas mean intensity (AU)
Cas^mSc mean intensity (AU)
YFP-VCL mean intensity (AU)
siCtrl
siSrc
siFyn
siYes1
ns
C
Cas^mSc
YFP-VCL
DMSO
EHT1864
10 µm
Cas^mSc mean intensity (AU)
YFP-VCL mean intensity (AU)
median Δt1/2 (VCL-Cas) (s)
D
siCtrl
siCas
Rac1-2G FRET
mean Rac1-2G FRET
E
siYes1
siYes

Figure 7 – figure supplement 1

Controls and additional data showing SFK-Cas-Crk-Rac1 signaling regulates adhesion assembly

(**A-B**) Representative immunoblots of cell lysates from Cas^{mSc} MCF10A cells treated with (**A**) control, Crk, CrkL or Crk/CrkL siRNA or (**B**) control, Src, Fyn or Yes1 siRNA. (**C**) Images (ventral section) of Cas^{mSc} YFP-VCL MCF10A cells treated with control, Src, Fyn, or Yes1 siRNA and fixed after 30 min of spreading. Staining for Cas^{mSc} and pY410Cas (above) or Cas^{mSc} and YFP-VCL (below). (**D**) Mean areas of siSFK cells in (**C**). (**E**) Representative FRET ratio images (left) and quantification (right) of Rac1-2G biosensor MCF10A cells treated with DMSO or Rac1 inhibitor EHT1864 and imaged after 30 min spreading. (**F**) Mean areas of EHT1864-treated cells. All error bars represent mean and SEM and all P values by Mann Whitney U tests.

Figure 7 – figure supplement 1

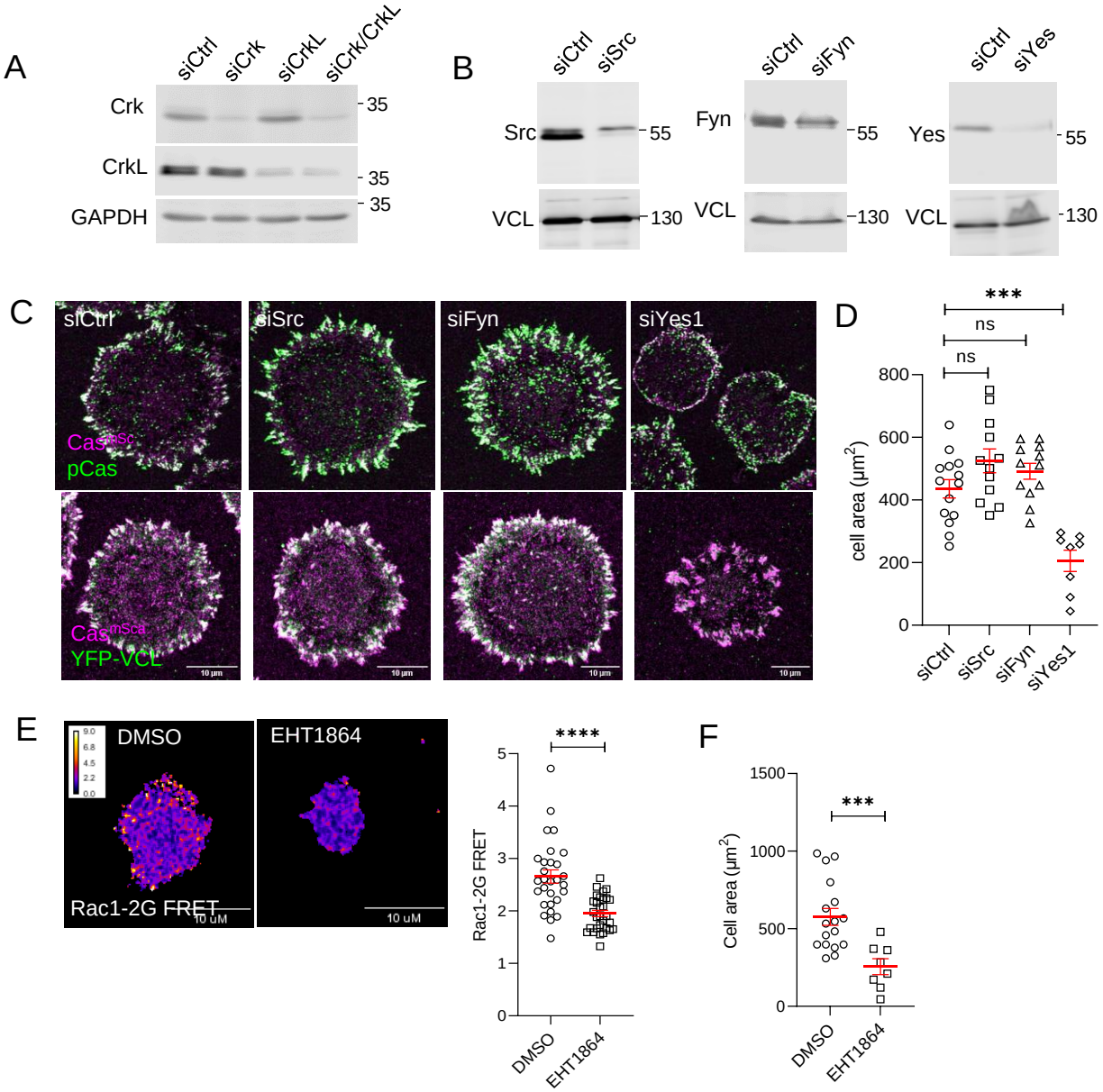

Figure 8

Linkage between cell spreading and adhesion assembly through positive and negative feedback

(**A**) Rac1 requires Cas to induce cell spreading. Representative images (ventral section) (left) and area quantification (right) of MCF10A cells transiently expressing EGFP-Rac1WT or -Rac1Q61L that were treated with control or Cas siRNA and fixed after 30 min of spreading. (**B-C**) NADPH-dependent oxidase inhibitor DPI inhibits Rac1 activation, cell spreading and vinculin recruitment to Cas clusters. (**B**) Representative FRET images (left) and quantification (right) of Rac1-2G biosensor MCF10A cells treated with DMSO or DPI and fixed after 30 min of spreading. (**C**) Representative endpoint dual color TIRF micrographs (left) and quantification (right) of 30 min spreading Cas^{mSc} YFP-VCL MCF10A cells treated with control or DPI. Graphs show mean cell area, mean Cas^{mSc} and YFP-VCL intensity, and median $\Delta t_{1/2}$ (VCL-Cas) from 7-12 cells in three biological repeats. (**D**) Inhibiting Cullins accelerates vinculin recruitment to Cas clusters. Representative endpoint dual color TIRF micrographs (left) and quantification (right) of 30 min spreading Cas^{mSc} YFP-VCL MCF10A cells treated with control or SOCS6 siRNA or with DMSO or Cullin Neddylation inhibitor MLN4924. Graphs show median $\Delta t_{1/2}$ (VCL-Cas) from 8-12 cells in three biological repeats. All error bars represent mean and SEM and all P values by Mann Whitney U tests. (**E**) Model showing nascent adhesions as sites of Cas clustering with inactive integrin, which leads to SFK-dependent phosphorylation of Cas, recruitment of Crk/CrkL, activation of Rac1 and ROS and positive feedback that strengthens and maintains signaling and recruits talin1, kindlin2 and other proteins to form a focal adhesion. This positive feedback is opposed by negative feedback resulting from SOCS6/cullin-mediated ubiquitination of phosphorylated Cas.

Figure 8

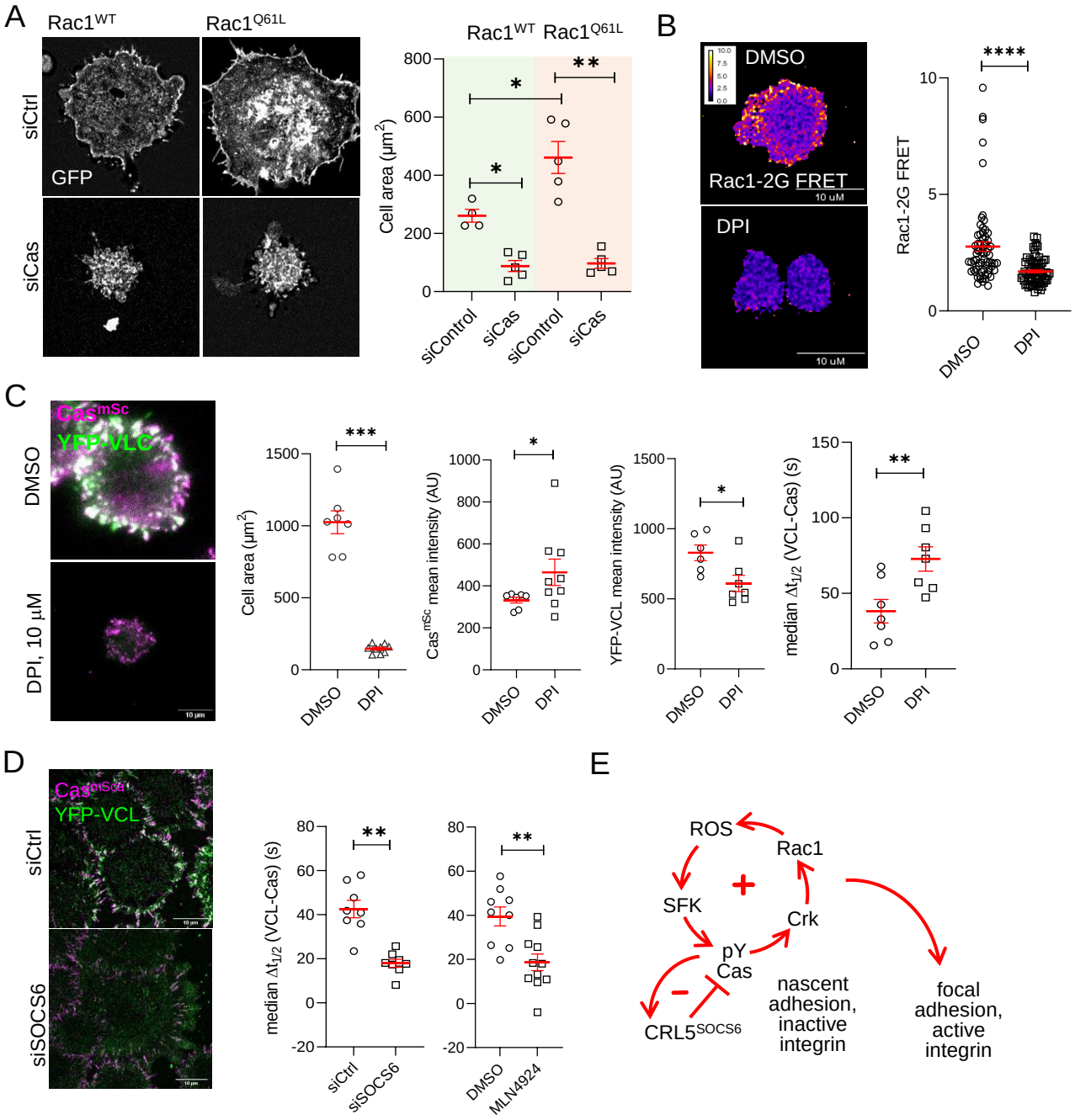
A
Rac1WT
Rac1Q61L
siCtrl
siCas
GFP
Rac1WT Rac1Q61L
Cell area (μm2)
siControl
siCas
siControl
siCas
B
DMSO
Rac1-2G FRET
10 uM
DPI
10 uM
Rac1-2G FRET
DMSO
DPI
C
CasmSc
YFP-VLC
DMSO
DPI, 10 μM
Cell area (μm2)
CasmSc mean intensity (AU)
YFP-VCL mean intensity (AU)
median Δt1/2 (VCL-Cas) (s)
DMSO
DPI
D
CasmSc
YFP-VCL
siCtrl
siSOCS6
median Δt1/2 (VCL-Cas) (s)
siCtrl
siSOCS6
DMSO
MLN4924
E
ROS
Rac1
SFK
Crk
pY
Cas
CRL5SOCS6
nascent
adhesion,
inactive
integrin
focal
adhesion,
active
integrin

Supplementary videos

Supplemental video 1 Cas (magenta) and vinculin (green) dynamics during attachment and spreading of a Cas^{mSc} YFP-VCL MCF10A cell on collagen. 15 s time intervals.

Supplemental video 2 Cas (magenta) and vinculin (green) dynamics during lamellipodia extension by a migrating Cas^{mSc} YFP-VCL MCF10A cell. 15 s time intervals.

Supplemental video 3 Quantification of Cas and vinculin cluster dynamics. MCF10A Cas^{mSc} YFP-VCL MCF10A cell spreading on collagen. (Left) Raw data. (Right) Regions of interest defined as regions of 20 pixels (0.5 μm^2) or greater in which either or both channel intensities exceed threshold in three consecutive frames. Regions are color coded according to the first frame in which the region is first detected, from cyan to magenta. 20 s time intervals.

Supplemental video 4 Effect of ECM. Cas (magenta) and vinculin (green) dynamics during attachment and spreading on collagen I (left) and fibronectin (right). 20 s time intervals.

Supplemental video 5 Integrin clustering. Cas (magenta) and integrin (green) dynamics during attachment and spreading. Left: Cas^{mSc} β1Ecto-pH MCF10A cell (20 s time intervals). Right: Cas^{mSc} $ITGB1^{GFP}$ HeLa cell (15 s time intervals).

Supplemental video 6 Cas-Crk dynamics. Cas (magenta) and Crk (green) dynamics during attachment and spreading of Cas^{mSc} Crk^{mGL} HeLa cells in presence of DMSO (left) or SFK inhibitor eCF506 (right). 20 s time intervals.

Supplemental video 7 Vinculin dynamics in control (left) and Cas-depleted (right) Cas^{mSc} YFP-VCL cells, 24 hr after plating on collagen. 20 s time intervals.

Supplemental video 8 SFK and Crk/CrkL requirement. Cas^{mSc} YFP-VCL MCF10A cells treated with DMSO (top left) or eCF506 (top right) or with siCtrl (bottom left) or siCrkL/CrkL (bottom right). 20 s time intervals.

Supplemental video 9 Rac1 and ROS requirement. Cas^{mSc} YFP-VCL MCF10A cells treated with DMSO (top left) or EHT1864 (top right) or with DMSO (bottom left) or DPI (bottom right). 20 s time intervals.

Supplemental video 10 Stimulation of vinculin recruitment and spreading in SOCS6-depleted cells. Cas^{mSc} YFP-VCL MCF10A cells treated with control (left) or SOCS6 (right) siRNA. 15 s time intervals.